Title Page

Theory, Investigation and Stability of Cathode Electrocatalytic Activity

Final Report

Reporting Period: 10/01/2008 – 9/30/2012

DOE Contract No.: DE-NT0006557

DOE Project Manager: Dr. Briggs White

Prepared by

Dong Ding, Mingfei Liu, Samson Lai, Kevin Blinn, and Meilin Liu

Center for Innovative Fuel Cell and Battery Technologies
School of Materials Science and Engineering
Georgia Institute of Technology
Atlanta, GA 30332-0245

Report Issued: January 2013

DISCLAIMER

ABSTRACT

The main objective of this project is to systematically characterize the surface composition, morphology, and electro-catalytic properties of catalysts coated on LSCF, aiming to establish the scientific basis for rational design of high-performance cathodes by combining a porous backbone (such as LSCF) with a thin catalyst coating. The understanding gained will help us to optimize the composition and morphology of the catalyst layer and microstructure of the LSCF backbone for better performance. More specifically, the technical objectives include: (1) to characterize the surface composition, morphology, and electro-catalytic properties of catalysts coated on LSCF; (2) to characterize the microscopic details and stability of the LSCF-catalyst (e.g., LSM) interfaces; (3) to establish the scientific basis for rational design of high-performance cathodes by combining a porous backbone (such as LSCF) with a thin catalyst coating; and (4) to demonstrate that the performance and stability of porous LSCF cathodes can be enhanced by the application of a thin-film coating of LSM through a solution infiltration process in small homemade button cells and in commercially available cells of larger dimension.

We have successfully developed dense, conformal LSM films with desired structure, composition, morphology, and thickness on the LSCF surfaces by two different infiltration processes: a non-aqueous and a water-based sol-gel process. It is demonstrated that the activity and stability of LSCF cathodes can be improved by the introduction of a thin-film LSM coating through an infiltration process. Surface and interface of the LSM-coated LSCF cathode were systematically characterized using advanced microscopy and spectroscopy techniques. TEM observation suggests that a layer of La and Sr oxide was formed on LSCF surfaces after annealing. With LSM infiltration, in contrast, we no longer observe such La/Sr oxide layer on the LSM-coated LSCF samples after annealing under similar conditions. This was also confirmed by x-ray analyses. For example, soft x-ray XANES data reveal that Co cations displace the Mn cations as being more favored to be reduced. Variations in the Sr-O in the annealed LSCF Fourier-transformed (FT) EXAFS suggest that some Sr segregation is occurring, but is not present in the annealed LSM-infiltrated LSCF cathode materials. Further, a surface

enhanced Raman technique was also developed into to probe and map LSM and LSCF phase on underlying YSZ substrate, enabling us to capture important chemical information of cathode surfaces under practical operating conditions.

Electrochemical models for the design of test cells and understanding of mechanism have been developed for the exploration of fundamental properties of electrode materials. Novel catalyst coatings through particle depositions (SDC, SSC, and LCC) or continuous thin films (PSM and PSCM) were successfully developed to improve the activity and stability of LSCF cathodes.

Finally, we have demonstrated enhanced activity and stability of LSCF cathodes over longer periods of time in homemade and commercially available cells by an optimized LSM infiltration process. Microstructure examination of the tested cells did not show obvious differences between blank and infiltrated cells, suggesting that the infiltrated LSM may form a coherent film on the LSCF cathodes. There was no significant change in the morphology or microstructure of the LSCF cathode due to the structural similarity of LSCF and LSM. Raman analysis of the tested cells indicated small peaks emerging on the blank cells that correspond to trace amounts of secondary phase formation during operation (e.g., CoO_x). The formation of this secondary phase might be attributed to performance degradation. In contrast, there was no such secondary phase observed in the LSM infiltrated cells, indicating that the LSM modification staved off secondary phase formation and thus improved the stability.

TABLE OF CONTENTS

1. INTRODUCTION

Solid oxide fuel cells (SOFCs) are potentially the cleanest, most efficient (especially when combined with turbines) chemical-to-electrical energy conversion systems with excellent fuel flexibility (i.e., potential for direct utilization of hydrocarbon fuels, coal gas, biomass, and other renewable fuels). Because of their ability to operate on fossil fuels as well as hydrogen, SOFCs could provide an economic bridge between the fossil-fueled economy and a hydrogen-fueled one [1-3]. Within the desired operating temperature range, however, the performance is often limited by the polarization resistance on the cathode side of the cell [4, 5].

A major goal in SOFC research is the development of cathodes with sufficiently low area-specific resistances (ASR). $La_{0.8}Sr_{0.2}MnO_3$ (LSM) is the most widely-used cathode for YSZ-based SOFCs because of its excellent chemical and thermal compatibility with YSZ; however, the catalytic activity of LSM is severely limited by its poor ionic conductivity (not by its surface catalytic activity as previously mistakenly believed), especially at low operating temperatures, so that the active sites for electrode reactions are limited mostly to the triple phase boundary (TPB) or near the TPB [6].

One of the reasons that $La_xSr_{1-x}Co_yFe_{1-y}O_{3-\delta}$ (LSCF) based cathodes show better performance than those based on $La_xSr_{1-x}MnO_{3-\delta}$ (LSM) is that LSCF has much higher ionic and electronic conductivity than LSM, significantly extending the active sites beyond the triple phase boundaries [7]. One obvious downfall for LSCF is that it reacts adversely with YSZ, which can be mitigated by the use of a buffer layer of doped-CeO_2 between LSCF and YSZ [8]. However, the performance of the stand-alone LSCF cathodes is likely to be limited by the surface catalytic properties [9]. Further, the long-term stability of LSCF cathodes is a concern. Thus, it is hypothesized that the performance and stability of a porous LSCF cathode may be improved by the application of a catalytically active coating on a LSCF backbone. This novel cathode could effectively combine the fast ionic transport of bulk LSCF with the rapid surface exchange reaction of a thin film. The selection of the catalytic materials as well as the detailed microstructures of the porous LSCF and the catalyst layer may critically impact the

performance of the proposed cathodes. Also, the demonstration of activity and stability improvement in commercially available cells will be a critical and final step to implement the application of the novel cathode in SOFC commercialization.

2. EXECUTIVE SUMMARY

We have successfully developed solution infiltration processes for deposition of catalyst coatings on the surface of a state-of-the-art LSCF cathode. The morphology of the infiltrated catalyst can be a continuous film or a dis-continuous coating of discrete particles, depending on the specific infiltration processes and catalyst materials. For example, we fabricated dense, conformal LSM films with the desired structure, composition, morphology, and thickness on LSCF cathodes in cells of different configurations. It is demonstrated that the activity and stability of the LSCF cathodes can be enhanced by the introduction of a thin-film LSM coating through an infiltration process. The surface and interface of the LSM-coated LSCF cathode were carefully characterized using advanced microscopy and spectroscopy techniques, including XRD, SEM, TEM, XAS, and Raman. Modeling and simulation were used for designing testing cells and understanding of mechanisms of LSM-coated LSCF cathodes with respect to enhancement in activity and stability. Based on the knowledge of LSM infiltration we obtained, a thin-film coating of $Pr_{1-x}Sr_xMnO_{3-\delta}$ (PSM) and $PrSrCoMnO_{5+\delta}$ (PSCM) were successively developed and they offered even higher activity than the LSM-infiltrated cells using both symmetrical and anode-supported cells. In addition, novel catalyst coatings in the form of discrete particles (e.g., SDC, SSC, and LCC) were successively developed to enhance the stability and activity toward oxygen reduction of the LSCF cathodes. Further, LSM infiltration process was also optimized for commercially available cells to demonstrate the enhancement effect in practical cells over longer periods of time. The significant findings can be briefly summarized as follows:

- Developed and optimized a non-aqueous sol-gel process and a water-based solution infiltration process for fabrication of LSM coatings on flat LSCF substrates and porous LSCF cathodes. The important process parameters include the amount of surfactant, pH value and concentrations of the solution, ambient humidity, and thermal treatment conditions.
- Quantified the correlation among performance, infiltration concentration and operating condition (polarization current density) in LSM-coated LSCF cathode; characterized porous LSCF and LSM-coated LSCF cathode electrochemically in terms of different time of polarization and relaxation as well as varied oxygen partial pressures.
- Demonstrated that the activity and stability of LSCF cathodes can be improved with a thin LSM film coating using cells of different configurations: thin film cells, symmetrical cells, and anode-supported button cells.
- Characterized the detailed structure, composition, and morphology of the LSCF surfaces and the LSM/LSCF interfaces under different conditions: (i) as prepared, (ii) after annealing at 850^{o}C for more than 900 hrs, and (iii) under conditions similar to fuel cell operation (active dc polarization).

- Characterized the atomistic and electronic structure of Co, Mn, and Sr in LSCF cathode with and without LSM coating at 850^{o}C annealed for 400 hours using synchrotron-based X-ray absorption spectroscopy (XAS).
- Developed a general and empirical method for designing thin-film test cells based on continuum modeling.
- Developed a semi-empirical phenomenological model for studying the mechanism of performance enhancement of the LSM coated LSCF cathodes. The results showed that that LSM coating is less active at open circuit voltage because it has fewer oxygen vacancies. However, it becomes more active under mild cathodic bias due to its larger relative increase in vacancy concentration under large cathodic bias as well as its suspected more favorable adsorption properties. These trends in the modeling agree with our experiments in both thin-film and porous operational cathodes.
- Developed new catalysts such as $Sm_{0.2}Ce_{0.8}O_{1.95-\delta}$ (SDC), $La_{0.4875}Ca_{0.0125}Ce_{0.5}O_{2-\delta}$ (LCC), and $Sm_{0.5}Sr_{0.5}CoO_{3-\delta}$ (SSC) to modify the LSCF cathode through a particle deposition process.
- Developed new Mn-based catalysts for infiltration into porous LSCF cathode, and demonstrated that infiltration of a thin-film coating of $Pr_{1-x}Sr_xMnO_{3-\delta}$ (PSM) and $PrSrCoMnO_{5+\delta}$ (PSCM) offered even higher activity than the LSM-infiltrated cells using both symmetrical and anode-supported cells.
- Established a new multi-cell testing stand for performance evaluation of the several commercial cells under the same conditions at the same time.
- Optimized the infiltration process for MSRI cells by adjusting the ratio of ethanol to water to tailor the wetting property of the solution; by controlling pH value to ensure the stability of the solution; by adopting QPAC as a sealant to prevent the solution from spreading out over the cathode area, enhancing the control of solution loading without introducing additional contamination; by applying a pre-infiltration thermal treatment process for MSRI cells to achieve better spreading of more concentrated LSM solutions; by investigating the concentration effect (0.05 M, 0.1 M and 0.3 M) of LSM solutions (at a fixed volume of 35 μL) infiltrated into the MSRI cells. Demonstrated that 0.3 M LSM solution was the optimal for improvement in performance, as confirmed by electrochemical testing for ~100 hours.
- Demonstrated enhanced activity and stability in commercially available cells at 750^{o}C with a constant voltage of 0.7 V.
- Developed a unique microstructure for dense continuum catalyst film on porous LSCF cathodes, which may suppress surface segregation of Sr in the LSCF cathodes.

3. EXPERIMENTAL

This study includes the development of processing procedures for fabricating thin-film catalysts (e.g., LSM or other new Mn-based materials) on LSCF; characterization of the morphology, composition, and catalytic activity of these materials under realistic operating conditions; identification of the correlation between catalytic activity and morphology/composition as well as their evolution over time; investigation into the polarization behavior and the chemical compatibility (or inter-diffusion) of the "buried" interfaces between the catalysts and the backbone under realistic operating conditions; application of our electrochemical models to the quantitative design of experiments, to the interpretation of experimental results, to the prediction of electrode performance, and to the design of new electrode structures/architecture; integration of gained knowledge into models and simulations to guide rational design of efficient cathode materials and structures of low loss and high stability; application of the knowledge to actual cells with the state-of-the-art LSCF-based cathodes, and validation of the theory and models using commercially available cells.

In order to optimize our infiltration process, we studied the relationship between a series of important parameters and the morphology and microstructure of LSM coating. In order to facilitate the electrochemical evaluation of LSCF cathode with and without LSM infiltration, we used symmetrical cells with three electrode configuration and applied a steady-state polarization to investigate the overpotential dependence of interfacial polarization resistance (Rp) in cathodes. We also used these cathodes in the homemade full cells to study the long-term stability under a constant voltage (0.7 V). Also, scanning electron microscopy (SEM), transmission electron microscopy (TEM), x-ray absorption spectroscopy (XAS), and Raman spectroscopy are employed to investigate the interface of cathode and the structural changes under the influence of external stimuli. The detailed structure, composition, and morphology of the LSCF surface and the LSM/LSCF interfaces in LSM-coated LSCF substrate were characterized using electron microscopy (SEM and TEM) and spectroscopy. Soft x-ray spectroscopy uses photons with energies on the order of a few 100 eV to probe the L-edge absorption of the different

transition metal cations, which provides useful information about the bonding and electron orbital occupancy. Hard x-ray spectroscopy was conducted using x-ray photons with energies ranging from 6 to 17 keV to probe the K-edge absorption and local atomistic structures of Co, Fe, Mn, and Sr. The microscopic details of the cathodes are also to be correlated directly with their electrochemical performance. Furthermore, a general and empirical method for designing test cells, and a semi-empirical method based on continuum modeling were developed for the interpretation of electrochemical testing results regarding the performance enhancement of the LSM-coated LSCF cathode.

In the case of water-free LSM infiltration, The LSM sols with different concentrations were prepared by dissolving proper amounts of $La(NO_3)_3 \cdot 6H_2O$, $Sr(CH_3COO)_2$, $Mn(CH_3COO)_2 \cdot 4H_2O$ (all 99.9%, Aldrich Chemical Co.,Milwaukee, WI, USA) in mixed solvents at room temperature. In the case of LSM, PSM and PSCM infiltration, stoichiometric amounts of high-purity praseodymium nitrate hydrate, lanthanum nitrate hexahydrate, strontium nitrate, cobalt nitrate hexahydrate, and manganese nitrate hydrate (all from Alfa Aesar) were dissolved in a mixture of deionized water and ethanol (at a volume ratio of 1:1) to form the solutions with different concentrations. 5 wt.% polyvinyl pyrrolidone (PVP) were added to the solution as a surfactant and stoichiometric amount of glycine were added as a complexing agent and the fuel for subsequent self-combustion. In the case of SDC, SSC, LCC infiltration, aqueous nitrate solutions of SDC, LCC and SSC precursors with different concentrations were prepared by dissolving proper amount of $La(NO_3)_3 \cdot 6H_2O$, $Ca(NO_3)_2 \cdot 4H_2O$, $Ce(NO_3)_3 \cdot 6H_2O$ and glycine into the distilled water. Glycine was used as a complex agent to facilitate the phase formation. In all infiltrations, 5 μL of the stock solution was deposited on the as-prepared LSCF surface or a porous cathode (0.3 cm^{-2}) using micro-liter syringe to control the amount of loading. The infiltrated cell was then fired at 900^{o}C for 1 h to get the desired phases after drying.

The effects of catalyst infiltration on the performance of the LSCF cathodes were investigated using symmetrical and anode-supported button cells. In the configuration of a symmetrical cell, YSZ pellets were prepared by uniaxially pressing a commercially available YSZ powder (Daiichi Kigenso, Japan) followed by sintering at 1450^{o}C for 5 h to achieve relative density of ~98%. LSCF (Fuel Cell Materials, US) green tapes were

prepared by tape-casting, which were then bound onto both sides of a YSZ electrolyte pellet using a slurry of $Sm_{0.2}Ce_{0.8}O_{2-\delta}$ (the buffer layer). The SDC powder was synthesized using a chemical co-precipitation process [10, 11]. The SDC powder was then dispersed in acetone with V-006 (Heraeus, US) as binder and ball-milled for 24 h to form a stable SDC slurry. The cells were then co-fired at 1080^{o}C for 2 h to form porous LSCF electrodes (with an area of 0.3 cm^2) on YSZ. The symmetrical cells were also tested in a three-electrode configuration. The LSCF cathode with/without catalyst coating were used as working electrode (WE) and counter electrode (CE), respectively. Pt paste was fired at 900^{o}C for 1 h as reference electrode (RE) by positioning it as close to working electrode as possible. In the configuration of an anode-supported cell, Tape-cast NiO/YSZ anode-support was first fabricated and pre-fired at 850^{o}C for 2 h. Then, an active NiO/YSZ layer (~15 μm) and a YSZ electrolyte (~15 μm) were sequentially deposited on the anode support by a particle suspension coating process followed by co-firing at 1400^{o}C for 5 h [38]. The cell size is about 1 mm in diameter. The LSCF cathode was then applied to the YSZ electrolyte using the same procedures as described in the fabrication of symmetric cells. The commercial button cells provided by MSRI are 27 cm in diameter with an active cathode area of 2 cm^2. The cell configuration is a conventional anode (NiO/YSZ)-supported electrolyte (YSZ) film. LSCF is used as the cathode material while SDC is employed as a barrier layer between electrolyte and cathode. LSCF/SDC is the cathode interlayer between LSCF and barrier layer. The infiltration processes were optimized by adjusting the composition of the solvent, pH value of the solution, and modifying the surface properties of the cathode. To accurately control the LSM loading, we applied poly-(alkylene) carbonates (QPAC) to prevent the solution from spreading outside the LSCF cathode. To maximize the performance improvement, we used LSM solution with different concentrations at a fixed volume to infiltrate the commercial cells. A short-term electrochemical test was performed on the infiltrated cells for ~200 hours, to comparatively study the extent of performance enhancement. When a series of optimal infiltration parameters were determined, a long-term electrochemical characterization at a constant voltage of 0.7 V at 750^{o}C was performed to observe the durability of the commercial cells with and without LSM infiltration. After testing, SEM was employed to investigate the surface, bulk, and interface of the cathode. The detailed structure and

morphology of the LSCF cathode were characterized. Also, the phase and structure of the cathode were analyzed by Raman spectroscopy [12].

4. RESULTS AND DISCUSSIONS

4.1 Development and Optimization of LSM solution infiltration

To better study the infiltration process and maximize the activity and stability enhancement, we successfully developed dense, continuous LSM films with desired structure, composition, morphology, and thickness on LSCF surface by two kinds of solution infiltration processes: a non-aqueous sol-gel process and a water-based process. In the former approach, 2-methoxyethanol and acetic acid were used to replace water as solvents, and strontium acetate and manganese acetate as metal organic precursors to replace nitrate precursors. The water-free LSM sol showed improved wettability on the LSCF surface. Actually, many solvents were examined in this study, including ethanol, i-propanol, n-propanol, ethylene glycol, 1,3-propanediol, 2-methoxyethanol, and acetic acid. Among them, 2-methoxyethanol and acetic acid appears the best. The volume fraction of acetic acid in the solvent mixture was stability and wettability of the sol. varied from 0 to 2/3, with 1/3 being the best to optimize the stability and wettability of the sol. The continuous and dense LSM films on LSCF substrates were fabricated, as shown in Figure 1.

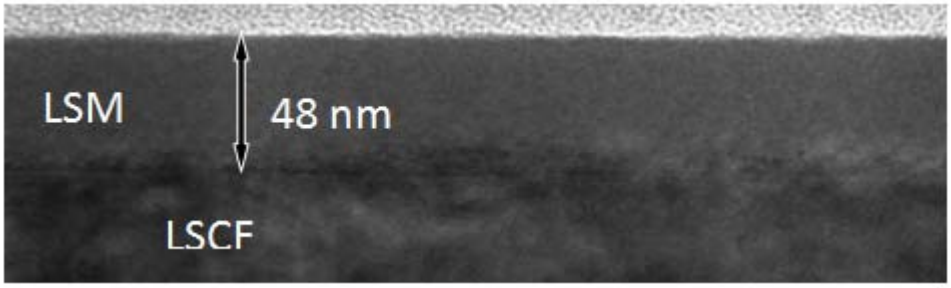

Figure 1 Cross-sectional TEM micrograph of LSM-coated LSCF surface derived from a sol-gel process on LSCF pellets annealed at 850^{o}C for 900 hours.

The identical infiltration process was applied to porous LSCF cathode. Due to the structural similarity of LSM and LSCF, it is hard to observe formation of the dense film or coating, as seen in Figure 2. Carefully analysis of cross-sectional TEM images indicates an epitaxial relationship of LSM with the underlying LSCF cathode.

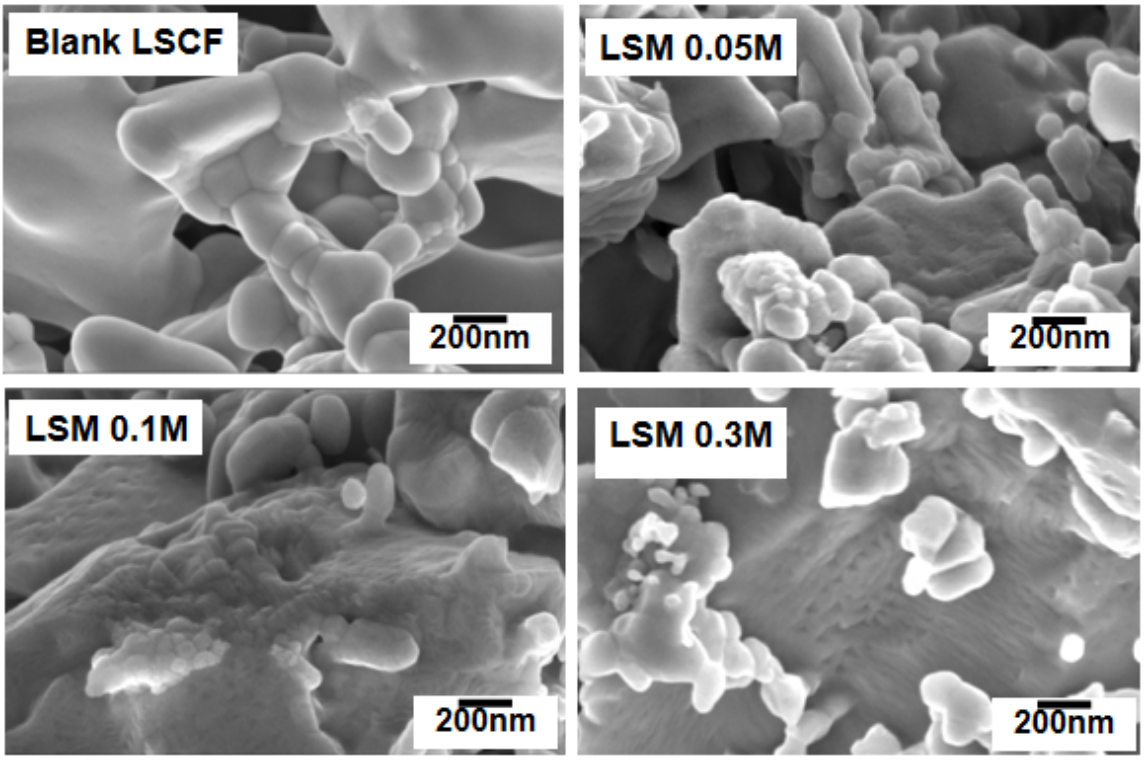

Figure 2 Microstructure of porous LSCF cathode with a sol LSM solution infiltration at different concentrations.

A water-based LSM infiltration process was also developed. Several process parameters have been demonstrated to have critical effects on the ultimate quality of LSM films, including solution pH value, surfactant type and amount. The results showed that a solution with 0.05 wt.% polyvinyl pyrrolidone (PVP) (among polyvinyl alcohol (PVA) and polyethylene glycol (PEG, molecular weight~4000)) and pH value of 0.3 is the best to obtain stable solution, and achieve dense and crack-free films. The ultimate objective was to maximize the enhancement in the electrocatalytic activity and stability of the LSM-coated LSCF cathode through proper control of the infiltration process. Figure 3 shows the change in current density with time of the blank cell and the LSM-infiltrated cell (home-made) under a constant voltage of 0.7V at 750^{o}C. The cell with LSM-infiltrated LSCF cathode initially had lower performance than the cell with blank LSCF cathode. However, the cell displayed a time-dependent activation that led to a considerable increase in performance in the first 200 h of operation. This increase contrasts with the rapid decrease in performance of the blank LSCF cell in the same time

period, suggesting that both power output and stability have been enhanced by the LSM infiltration.

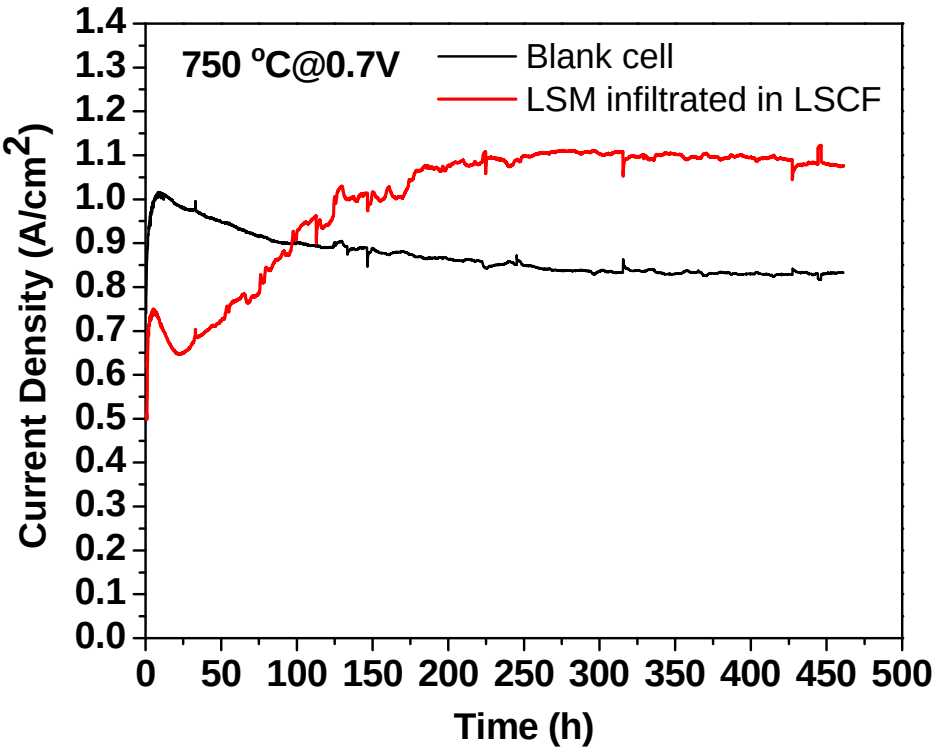

Figure 3 Typical current output of home-made button cells with a blank LSCF and an LSM infiltrated LSCF cathode at 750°C with a constant voltage of 0.7 V.

To investigate the electrochemical behavior of LSM infiltrated porous LSCF cathodes at different cathodic polarization conditions and correlate the performance with the LSM infiltration solution concentration (to which the coating thickness should be proportional), a series of direct current (DC) passage treatments were applied to symmetrical cells with a three-electrode configuration and their relevant steady polarization behavior was examined. Shown in Figure 4 is a comparison in interfacial polarization resistance (R_p) for a blank LSCF and an LSM-infiltrated LSCF cathode with different concentrations of LSM solutions measured at different cathodic current densities. Obviously, the R_p of all of the infiltrated LSCF cathodes are larger than that of the blank LSCF under the open circuit voltage condition, and they increase with solution concentration. When a cathodic current was passed through the cell, the R_p in all cases

decreased. The higher the infiltration solution concentration, the larger the decreasing rate. If the current density is high enough (e.g. 1 A cm^{-2}), the R_p for all of the infiltrated LSCF cathodes show similar values which were visibly lower than that of blank LSCF cathode under the same conditions. Accordingly, it seems there is a compromise between performance improvement and solution concentration under different operating conditions.

A typical comparison for the interfacial polarization resistance (R_p) for LSCF cathodes with and without LSM infiltration is shown in Figure 4. Clearly, the R_p for LSM infiltrated LSCF cathode decreases much faster than that for blank LSCF cathode with increasing cathodic polarization, leading to smaller R_p at higher polarization in spite of the initially larger value in the former. This is the reason that the performance of an LSM-infiltrated LSCF cathode is enhanced under typical fuel cell operation conditions.

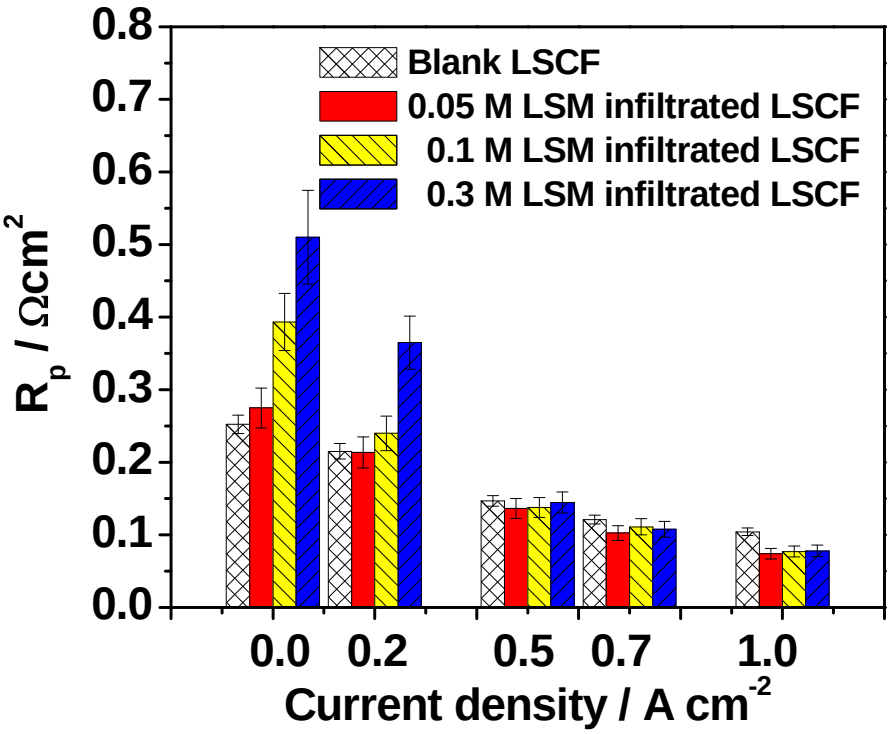

Figure 4 Interfacial polarization resistance versus cathodic current density for LSCF cathodes without/with 0.05, 0.10 M, and 0.30 M of LSM infiltration measured at 750°C. Impedance spectra were obtained with a steady state polarization with a constant cathodic current passage.

4.2 Surface and Interface study of LSCF and LSM/LSCF

Dense LSCF pellets were prepared by uniaxially pressing LSCF powders (Fuel Cell Materials, US) followed by sintering at 1350^{o}C for 5 h to achieve relative density of ~98%. After grinding and polishing,, LSM solution was coated on the polished surfaces of the LSCF pellets, producing an LSM film with thickness ranging from 42 nm to 50 nm. Subsequently, the samples were annealed at 850^{o}C for 900 hours to examine microstructure evolution. Advanced electron microscopy and spectroscopy were used to examine the morphology, composition, and structure of the LSCF surfaces as well as the LSM/LSCF interface before and after long-term annealing to understand the stability enhancement of the LSM-coated LSCF cathode. The blank LSCF pellet after annealing at 850^{o}C for 900 hours was firstly examined. Figure 5 presents a bright-field STEM image of the surface of an LSCF pellet after annealing at 850^{o}C for 900 hours. The sample was coated with a thin layer of Cr to provide delineation of the sample surface, and then prepared using focused ion beam (FIB). EDS profiling was performed from the surface of the annealed pellet to a depth of about 1.7 μm as shown Figure 5(b), with a 1-nm probe along a line marked by the rightmost arrow in Figure 5(a). EDS quantification was calibrated with commercial 6428LSCF powder. The profiles show a uniform composition of LSCF over the entire depth within LSCF. The LSCF composition averaged within LSCF (under the surface La-Sr-oxide/LSCF interface or equivalently from about 200 nm to 1.7 μm) is 12% La, 8% Sr, 5% Co, and 15% Fe, which is very close to 12% La, 8% Sr, 4% Co, and 16% Fe for 6428LSCF. On the surface, only La and Sr were detected.

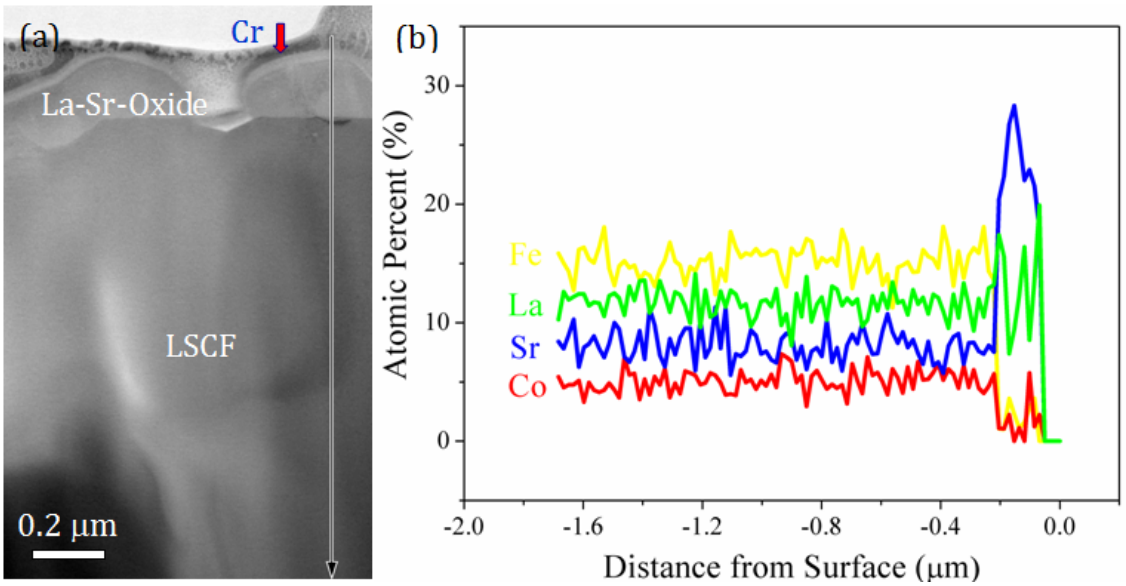

Figure 5 Bright-field STEM image of surface of an LSCF pellet annealed at 850°C for 900 hours. A thin layer of Cr coating was used to delineate the sample surface. The rightmost arrow indicates the EDS profile line. (b) Atomic percent profiles acquired along the profile line marked in (a).

As a sharp contrast, Figure 6(a) shows the cross-sectional view (TEM image) of a LSM film deposited surface layer in the as-deposited state on a dense LSCF pellet, while Figure 6(b) shows the cross-sectional view of a similar surface layer after annealing at 850°C for 900 h (under zero-current conditions). Figure 6(c) and (d) show EDS composition profiles of the surface layer and outermost portion of the underlying LSCF in the as-deposited state and in the long-term annealed state, respectively. The surface layer retains Mn during long-term annealing but also experiences an addition of Co. These TEM observations suggest the formation of a thick oxide of La and Sr after annealing on the blank LSCF pellet (and possibly along the LSCF grain boundaries on the LSM-coated LSCF pellet where Mn is largely absent). As a sharp contrast, there is no such thick oxide on the LSM-coated LSM after annealing. Such thick surface oxide particles are expected to severely hamper electrochemical activities but have not emerged on LSM-coated surface of LSCF after annealing.

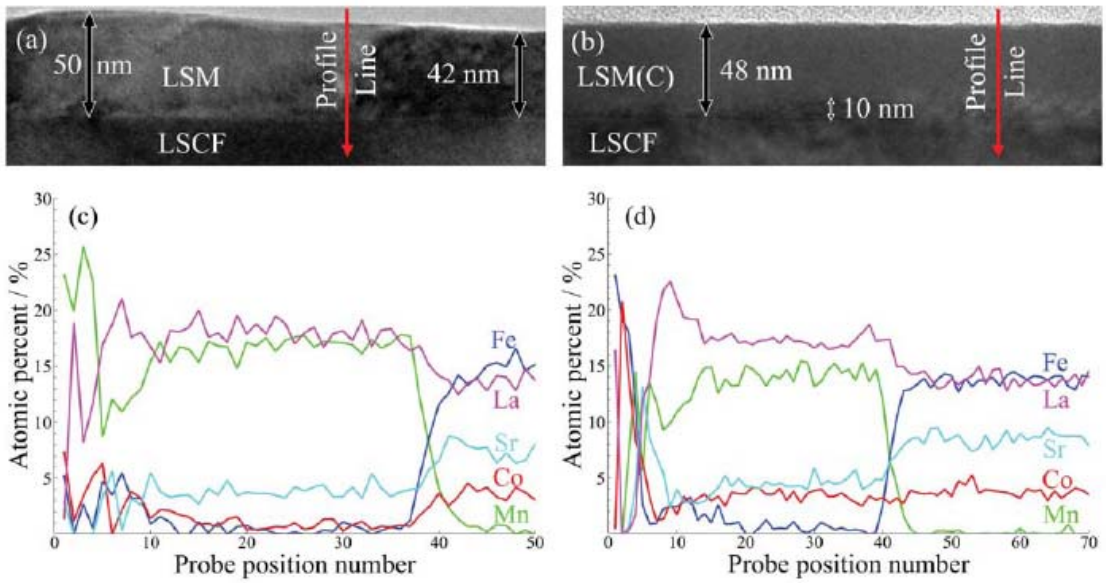

Figure 6 Cross-sectional TEM micrograph of a LSM-modified LSCF surface a) in the as-deposited condition and b) after long-term annealing at 850°C for 900 h. EDS compositional profiles across the sol–gel surface layer and outermost part of LSCF layer c) in the as-deposited condition and d) after long-term annealing.

Figure 7(a) is a TEM image of an LSCF grain in the LSM-infiltrated cathode subjected to 900 hours of operation. Presented in Figure 7(a) are some typical performances of the cells with LSCF cathodes (with and without LSM modification). The LSCF grain maintains the perovskite structure, as revealed by its lattice fringes deep in the bulk and at the edge of the LSCF grain in Figure 7(a)-(e). The surface layer contains all the cations of LSCF and LSM. Thickness of the surface layer ranges from 2 to 23 nm as shown in Figure 7(a). The results suggest that the thickness of the LSM films on an LSCF pellet was largely preserved during annealing at 850ºC for 900 hours. However, it appears that Mn migration along the LSCF grain surface, combined with the evolution of LSM on the LSCF grain, led to the formation of a thin layer of LSM that contained some Co. The degree of regularity of atom arrangement is also reduced (from long to short range order), which favors oxygen ion conductivity. On the other hand, the thickness of the LSM layer is very small, ranging from 2 to 23 nm. The small thickness is expected to ease transport of the oxygen ions to the LSCF.

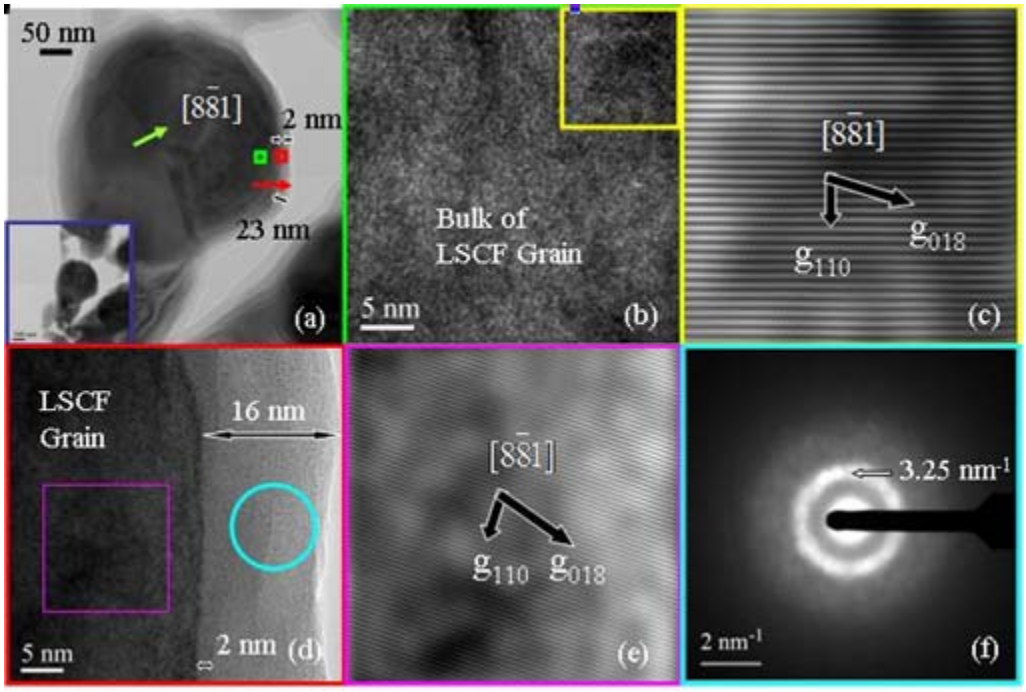

Figure 7 Microanalysis of porous LSCF cathode infiltrated with LSM after operation (under a constant cell voltage of 0.7V) at 750ºC for 900 hours. (a) TEM images of LSCF grain in the porous cathode infiltrated with water-based LSM solution and after 900 hours of operation at 750ºC. The color squares mark areas that were zoomed in and are displayed in (b) to (f). The color arrows denote profile lines. The inset provides a lower magnification image of the LSCF grain. (b) HRTEM image of the LSCF grain within the green square in (a). (c) Fourier-filtered image of the yellow square in (b). (d) HRTEM image of surface of the LSCF grain within the red square in (a). (e) Fourier-filtered image of the magenta square in (d). (f) Convergent beam electron diffraction from surface layer within the blue circle in (d).

4.3 Comparative study of LSM-infiltrated LSCF and blank LSCF cathode using X-ray absorption spectroscopy (XAS)

We employed X-ray absorption spectroscopy (XAS) to probe the atomistic and electronic structure of Co, Fe, Mn, and Sr in electrode materials. The goal was to directly correlate the electronic and structural changes on a particular cation or anion under the influence of external stimuli with the electrochemical response of the electrode under the same conditions. The soft x-ray absorption near-edge spectroscopy (XANES) data reveal that in the as-prepared LSM infiltrated LSCF at 750°C under ultra high vacuum, a strongly reducing condition, the Mn and Co cations are reduced by the charge imbalance caused by oxygen vacancy. However, if the LSM infiltrated LSCF was annealed *ex situ*

for 120 h at 900°C, only the Co cation is reduced. The Fe L-edge absorption did not exhibit significant changes in spectroscopic features.

The hard x-ray K-edge XANES indicate that in as-prepared LSM infiltrated LSCF, the Mn cation is reduced at 750°C, whether it is heated in oxygen or nitrogen, while the Co cation is unaffected. However, when the LSM infiltrated LSCF is annealed for several hundred hours, the spectroscopy shows that the Mn cation is unaffected by heating in oxygen or nitrogen while the Co cation oxidizes or reduces according to the change in the oxygen vacancy concentration. Thus, for the as-prepared cathode material, the charge compensation is mostly handled by the Mn cation, as shown by soft and hard x-ray spectroscopies. Unless the material is under sufficiently strong reducing conditions, such as at 750°C in ultra high vacuum, Co does not participate in electrochemical reactions. However, once the annealing process enables Co diffusion into the LSM thin film on the surface, the Co displaces Mn as the charge-compensating cation for changes in oxygen stoichiometry, an important change in the fundamental electrochemical reactions taking place. These results are partly summarized in Table 1.

Further investigation in the Mn and Co K-edge Fourier-transformed (FT) extended x-ray absorption fine structure (EXAFS) show that the local structures of both cations showed significant peak growth after brief thermal treatments and annealing, which indicates ordering of the coordination shells. The Fe, Co, and Sr K-edge FT EXAFS data indicate that the annealed LSM-infiltrated LSCF has local structures similar to as-prepared LSCF, which suggests that the LSM infiltration helped preserve the LSCF structure. In contrast, slight contractions were observed in the Fe-O, Co-O, and Sr-O coordination shells in the annealed LSCF without LSM infiltration. The oxidation state changes, the ordering phenomenon, and local structure contractions are observations uniquely obtained through the XAS technique and provide useful insight into the effects of thermal treatments and oxidizing and reducing atmospheres on structure and electronic state.

Sample	Mn	Co	Fe	Sr
As-prepared LSM infiltrated LSCF	Reduced (soft x-ray) Reduced (hard x-ray)	Reduced (soft x-ray) No change (hard x-ray)	No change	No change
Annealed LSM infiltrated LSCF	No change	Reduced (soft x-ray) Oxidized/Reduced (hard x-ray)	No change	No change

Table 1. A summary of the some of the important results obtained through soft and hard x-ray XANES. The shifts in the absorption energy describe oxidative or reductive changes in a particular cation.

4.4 Application of Surface Enhanced Raman Spectroscopy to the study of LSM-coated LSCF cathode in SOFC

The LSM-coated LSCF cathode achieved enhancements in activity and stability, which are possibly associated with effective modification agents and degradation-resistance species. They could be present in trace amounts, which become difficult to detect using conventional characterization tools because of the lack of chemical sensitivity, lack of surface specificity, or limited applicability under *in situ* conditions. Under the right conditions, Raman spectroscopy is able to inspect the phase evolution and reaction intermediates at the electrode surface [13, 14]. However, the inherently low chemical sensitivity of Raman precludes probing species present in trace amounts on the SOFC surface that are connected to cell performance. We successfully developed a DC magnetron sputtering method to load silver nanoparticles as the SERS agent, and obtained the enhanced Raman signal for LSM and LSCF films on a YSZ substrate [15]. As shown in Figure 8(a) and (b), the Raman spectra collected from both LSCF pellets and LSM thin film were significantly enhanced after SERS conditioning while normal Raman signals of both materials were very weak because near-cubic perovskite phases have little Raman activity. Since the two materials share a similar phase, their Raman bands are in similar positions. The LSCF signal was enhanced by a rough factor of ~ 11, and the LSM signal was enhanced by a factor of ~ 6. Moreover, the Ag treatment granted some level of surface specificity to the Raman analysis since only the signal from chemical species near the Ag nanoparticles is enhanced. This feature can provide the capability to detect phase evolution on the cathode surface with superior surface sensitivity, potentially contributing to studies on the degradation mechanisms of LSCF cathodes in SOFCs.

The enhancement in sensitivity of Raman spectroscopy to cathode materials has important implications. To date, the development of new electrode materials for SOFC is still largely based on experience and intuition rather than scientific models, largely due to the lack of a fundamental understanding of the electrode processes, which are determined by the chemistry and structure of electrode surfaces. We believe that SERS with high

sensitivity to electrode materials may be a powerful probe for surface composition and electrode structure, providing critical information for unraveling the mechanism of catalyst-coated LSCF cathode processes.

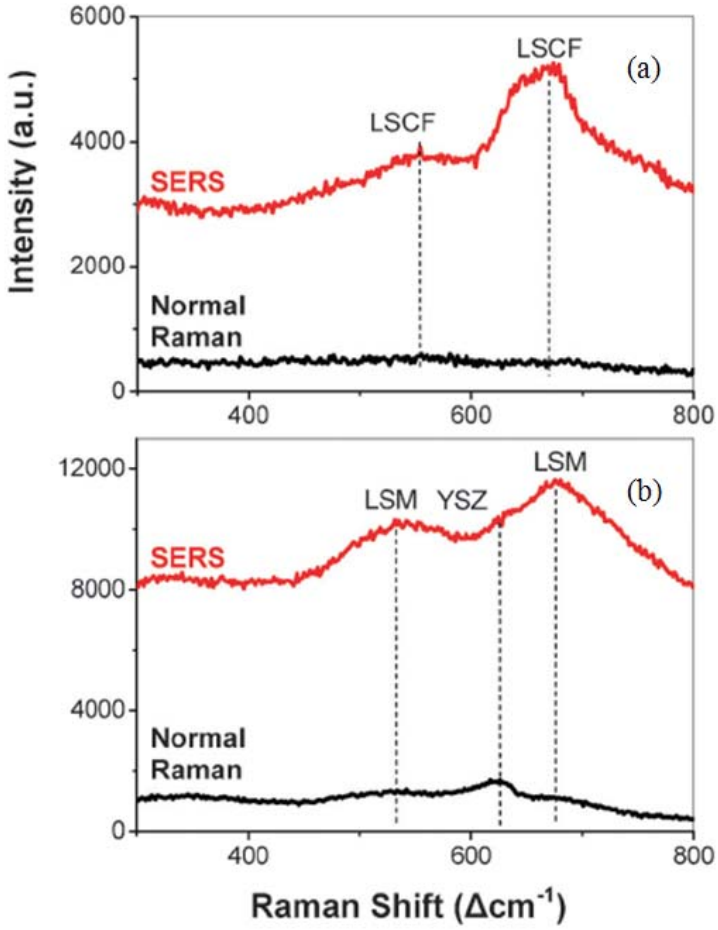

Figure 8 The normal Raman and SERS spectra collected from (a) an LSCF pellet, and (b) LSM film sputtered on a YSZ pellet. They were excited with a green laser (514 nm wavelength).

4.5 Modeling and simulation for LSM-coated LSCF cathodes in SOFCs

4.5.1 A general and empirical method for designing test cells

We have developed a model for evaluation of the sheet resistance in thin film working electrodes for the exploration of fundamental properties of the MIECs of interest. Figure 9(a) shows the alternating current solution of a distribution of RC parallel circuits over the surface of the film, solved for with different film conductance (the product of the film thickness t_m and the conductivity σ). At low film conductance, an extraneous high-

frequency feature appears in the impedance concomitant with an increase in the overall zero-frequency total resistance. This effect is detrimental and it must be avoided, and the only way to do that is to design test cells properly to limit sheet resistance. The empirical model was used to accomplish that task. Figure 9(b) shows a selection chart plotting the contour of the logarithm of the critical current collector spacing (in microns) for a particular current collector configuration leading to no more than a 0.5% increase in the total resistance as a function of the polarization resistance and film conductance. Such plots allow the determination of constraints upon a current collector in order to limit sheet resistance in a film. The ability to design and fabricate test cells with good thin-film working electrodes of acceptable sheet resistance is vital to evaluating the fundamental properties of LSCF and LSM thin films.

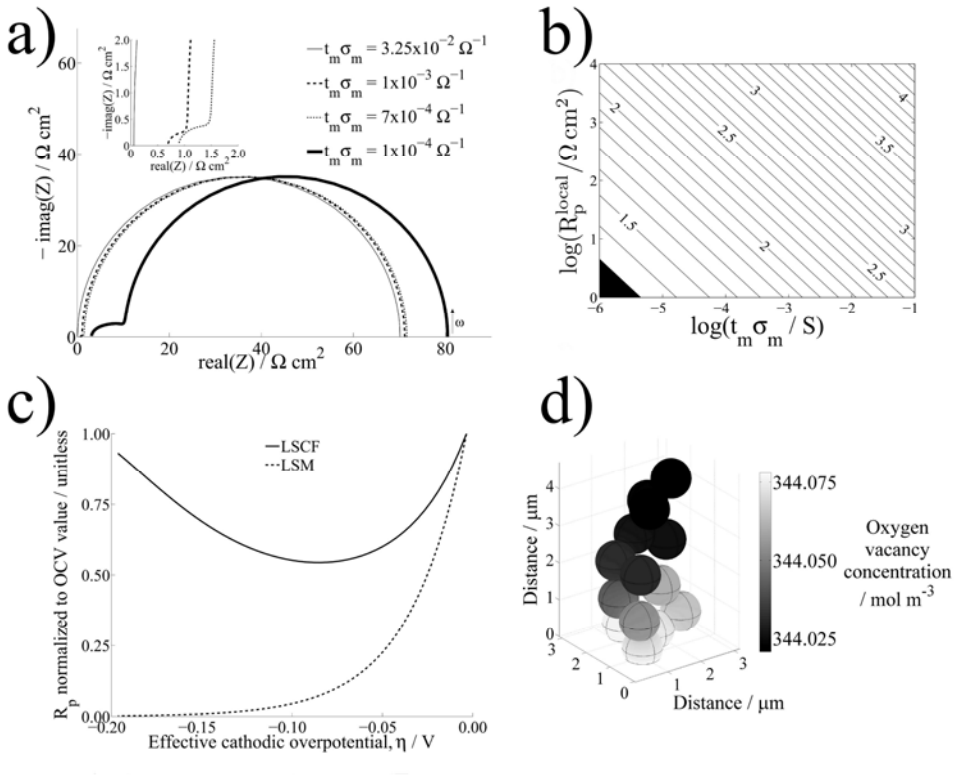

Figure 9 Key continuum modeling results: (a) Impedance response for different film conductance simulated using the empirical sheet resistance model for a simple RC circuit distributed over the film. (b) Generated charts for selecting the maximum current collector spacing for a discrete-contact current collector arrangement. (c) Polarization resistance of LSM and LSCF normalized to the OCV value simulated using the micro-kinetic model. (d) Oxygen vacancy distribution in the porous representation of LSCF.

4.5.2 A semi-empirical phenomenological model for mechanism of LSM-coated LSCF cathodes

We extended our model of the phenomenon of LSM-coated LSCF cathodes. Figure 10(a) shows the trend of the area normalized interfacial resistance modeled as a function of oxygen vacancy concentration dependent upon cathodic bias. LSCF clearly has a different trend from LSM, as it is suspected that the trend of LSM leads to improved performance under large bias when the LSM is coated with LSCF. Figure 10(b) shows the trend of interfacial resistance as oxygen vacancy formation is made less favorable by modifying the free energy of reaction. The trend shows an increasing tendency toward larger activation at more severe cathodic bias. Figure 10(c) and (d) show how the trend of the area-specific resistance is affected by making adsorption and dissociation of oxygen more favorable. These results indicate that the LSM coating is less active at open circuit voltage because it has fewer oxygen vacancies. However, it becomes more active under large cathodic bias because of a larger relative increase in oxygen vacancy concentration and its suspected more favorable adsorption properties under mild cathodic bias. These modeling trends agree with our experiments in both thin-films and porous, operational cathodes.

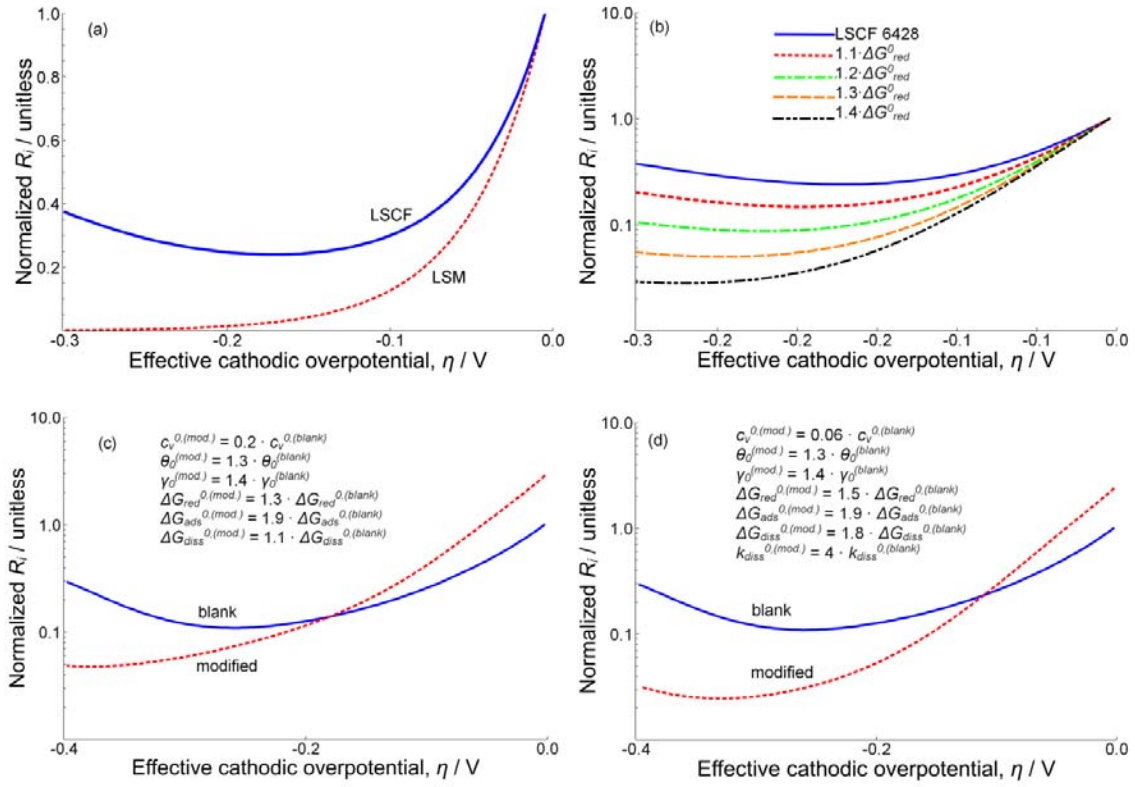

Figure 10 a) Normalized interfacial resistance of LSCF and LSM films assuming that the current at the effective overpotential is described by Equation $i \propto \left(\frac{C_v}{C_v^0} - 1 \right)$. Normalized to their respective values at OCV. b) Normalized interfacial resistance associated with tighter oxygen binding associated with lower free energy of oxygen reduction assuming current proportional to oxygen vacancy concentration. c) Simulated normalized interfacial resistance versus effective cathodic overpotential for blank LSCF and LSCF with modified surface properties when $\Delta G_{red}^{0(surface)} < \Delta G_{red}^{0(LSCF)}$, $\Delta G_{diss}^{0(surface)} < \Delta G_{diss}^{0(LSCF)}$, and $\Delta G_{ads}^{0(surface)} < \Delta G_{ads}^{0(LSCF)}$. R_i is normalized to the value of the blank LSCF at OCV. d) Simulated normalized interfacial resistance versus effective cathodic overpotential for blank and LSCF with modified surface properties when $\Delta G_{red}^{0(surface)} < \Delta G_{red}^{0(LSCF)}$, $\Delta G_{diss}^{0(surface)} < \Delta G_{diss}^{0(LSCF)}$, $\Delta G_{ads}^{0(surface)} < \Delta G_{ads}^{0(LSCF)}$, $k_{diss}^{0(surface)} > k_{diss}^{0(LSCF)}$.

4.6 Development of other novel electro-catalyst coatings (particle deposition)

We have developed methodologies for deposition of discrete nano-particles on an LSCF backbone. $Sm_{0.2}Ce_{0.8}O_{1.95-\delta}$ (SDC), $La_{0.4875}Ca_{0.0125}Ce_{0.5}O_{2-\delta}$ (LCC), and $Sm_{0.5}Sr_{0.5}CoO_{3-\delta}$ (SSC) were infiltrated into porous LSCF backbones. As shown in Figure 11, the LCC, SDC, and SSC nano-particle phases are formed after heat treatment at

900^{o}C with different infiltration concentrations, and they are uniformly distributed on the surface of LSCF grains. The typical SDC nano-particle size is in the range of 50-100 nm, which is much smaller than the 0.2 to 0.5 μm size of the LSCF grains of the pre-sintered LSCF electrode backbone. As shown in Figure 12, a significant improvement can be observed in activity of the cells with LCC, SDC, and SSC infiltration as well as in stability of the cell with LCC infiltration.

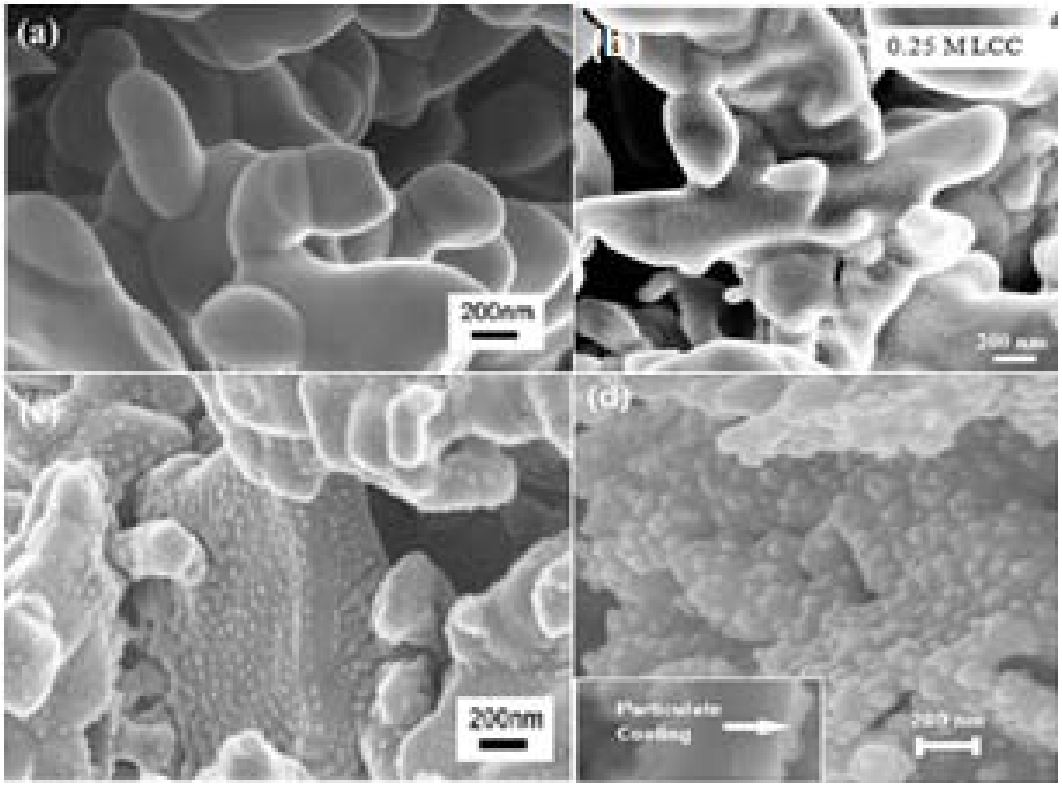

Figure 11 SEM images of the cross-section of LSCF cathodes: (a) blank LSCF; (b) LCC infiltration; (c) SDC infiltration, and (d) SSC infiltration.

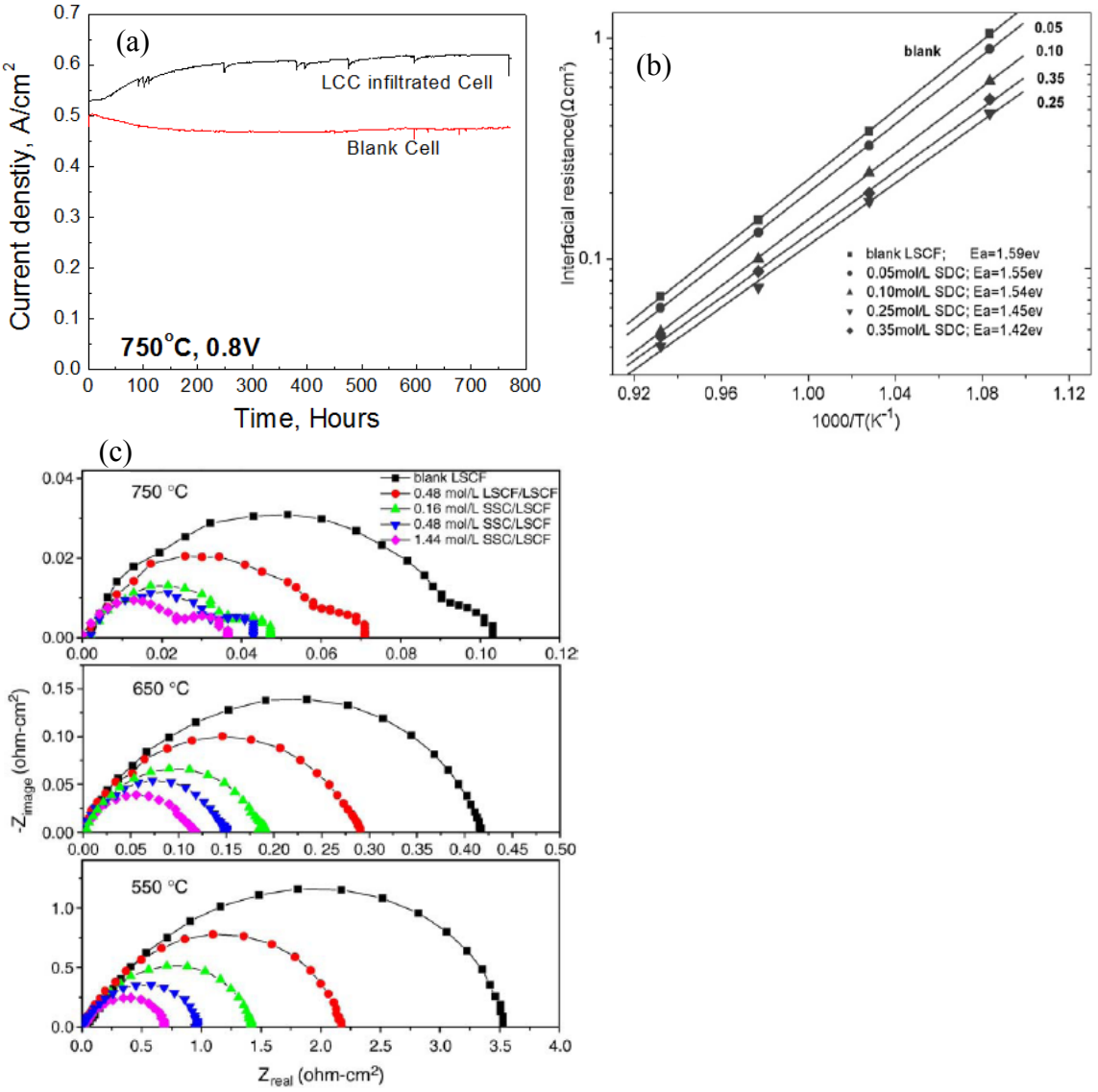

Figure 12 a) Typical lifetime of the homemade button cells with LCC-infiltrated LSCF as well as a baseline LSCF cathode under a constant voltage of 0.8 V at 750°C, b) temperature dependence of interfacial polarization resistance of blank LSCF cathode and LSCF cathode with different concentrations of SDC infiltration measured at OCV, and c) impedance spectra of LSCF cathodes with SSC infiltration at different concentrations

4.7 Development of novel Mn-based electro-catalyst coatings (continuous film coating)

Considering the general consensus that the degradation of LSCF cathode at high temperatures operation is primarily derived from SrO segregation or enrichment on the surface[8], a continuous dense thin film which coats the whole surface of the LSCF grain

would theoretically have the greatest potential to suppress the segregation or enrichment of SrO on the surface, thus mitigating that degradation mechanism. While LSM continuous thin film coatings were successfully demonstrated to provide activity and stability enhancement for LSCF cathodes, we attempted to infiltrate some new catalysts based on our obtained knowledge from LSM coating. The series of Mn-containing active catalysts for infiltration that were developed included: 1) simple perovskite $Pr_{1-x}Sr_xMnO_3$ (i.e., replacing La in LSM by Pr) and 2) complex perovskite PrSrCoMnO (i.e., substituting half of the Co in $PrBaCo_2O_{5+x}$ by Mn and replacing Ba in the A-site by Sr). Both PSM and PSCM are derivatives of a doped lanthanide manganite, a family of cathode materials widely studied for SOFC. The similarity in crystal structure of PSM and PSCM to that of LSCF (perovskite) allows for facile formation of a conformal coating on an LSCF surface, which has the potential to suppress SrO segregation or enrichment on the surface, thus enhancing stability and durability under operating conditions[16]. The choice of Pr in the A site was inspired by the superior oxygen exchange activity of this element in the $Ln_{1-x}Sr_xMnO_{3-\delta}$ and $LnSrCoMnO_{6-\delta}$ family of materials (where Ln represents the lanthanide elements from La to Gd)[17-19]. Perovskite cathodes with Mn in the B-site are known for their stability over long term operation while cobaltites show excellent ionic and electronic conductivities[20]. The aim of substituting cobalt in the B-site of the lanthanide manganite is to increase the catalytic activity without compromising the stability.

The electrochemical behavior of the catalyst-infiltrated LSCF cathodes was characterized at 750^oC under open circuit conditions using impedance spectroscopy (Figure 13(a)). Unlike the LSM-infiltrated LSCF cathode, which had a higher impedance than the blank LSCF cathode, the PSM-infiltrated LSCF cathode displayed smaller impedance than the blank LSCF cathode. Clearly, the PSM-infiltrated LSCF has higher catalytic activity for the ORR than the LSM-infiltrated LSCF cathodes. The PSM coating significantly reduced the interfacial R_p of the LSCF cathode even under open circuit voltage condition, in contrast to the LSM infiltration. The PSCM infiltration further decreased R_p at the same concentration of infiltration. Figure 13(b) shows the temperature dependence of R_p for these catalyst-infiltrated LSCF cathodes. At an intermediate temperature range, the PSCM infiltration provided the lowest R_p among

these Mn-containing catalysts. All of the curves appear to have similar slopes, indicating that the primary ORR mechanism remains the same.

We employed symmetrical cells with a three-electrode configuration to evaluate the polarization behavior. Unlike LSM infiltration, the PSM and PSCM infiltrated LSCF cathodes initially showed lower R_p compared to blank LSCF cathodes (Figure 13(c)), followed by a fast reduction in R_p at a given cathodic overpotential. This suggests that PSM and PSCM infiltration are able to further enhance performance under operating conditions. Shown in Figure 13(d) is the typical performance of button cells infiltrated with different catalytic coatings and operated at 750^{o}C under a constant cell voltage of 0.7 V. Within 550 hours, the cells with the PSCM-infiltrated LSCF cathodes showed the best performance with significant activation behavior. Compared to the cells with LSM and PSM infiltration, the PSCM infiltrated cells showed a gradual increase in performance, implying a continuous activation during operation. The "long-term activation" effect could counter against other degradation mechanisms and stabilize cell output. This phenomenon has attracted our attention for further study. Due to possible degradation of the blank LSCF cathode during operation, an even larger performance difference would be expected for operation over a longer period of time.

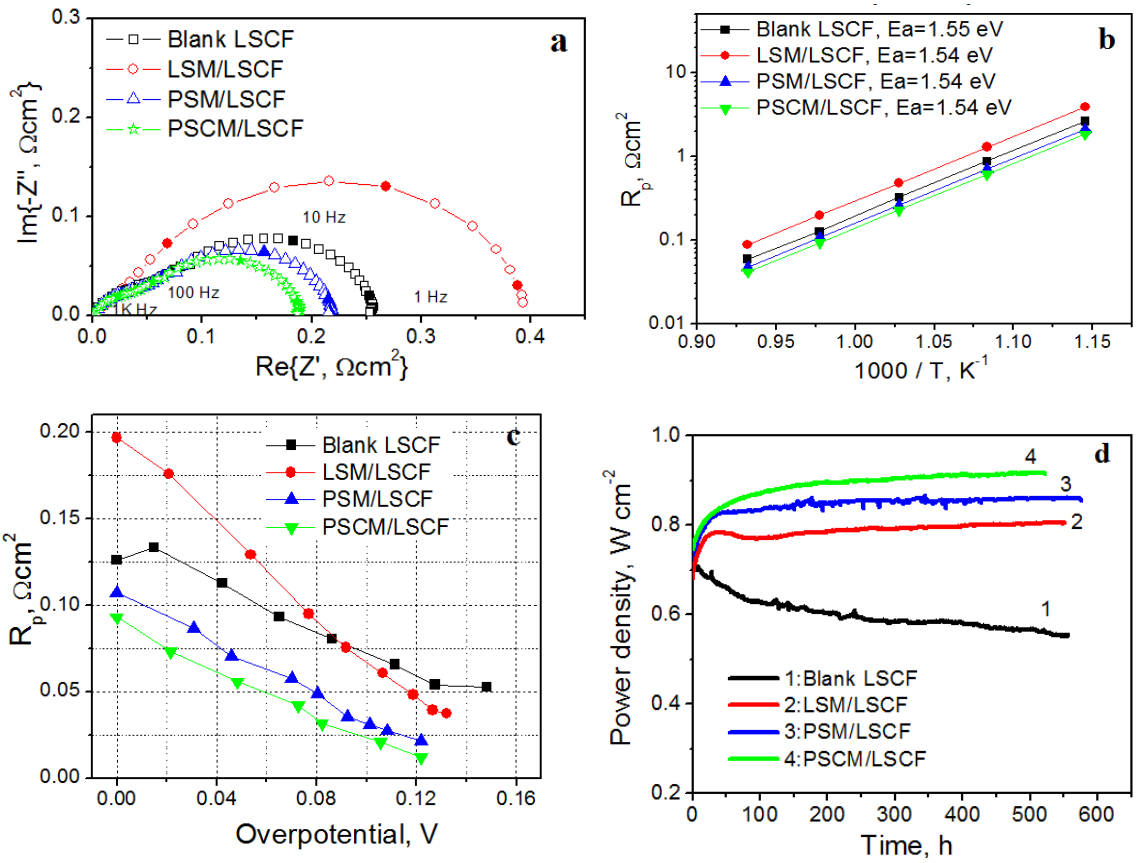

Figure 13 (a) Typical impedance spectra of catalyst-infiltrated LSCF cathodes measured at 750°C under open circuit (OCV) conditions; (b) temperature dependence of interfacial polarization resistance (R_p) of catalyst-infiltrated LSCF cathodes under OCV conditions; (c) interfacial polarization resistance (R_p) versus cathodic overpotential (η) for catalyst-infiltrated LSCF cathodes as measured at 750°C; and (d) power outputs of anode-supported cells with catalyst-infiltrated LSCF cathodes at a constant cell voltage of 0.7 V at 750°C with humidified H_2 (3 vol% water vapor) as the fuel and stationary air as the oxidant.

4.8 Demonstration of activity and stability enhancement in commercially available cells through LSM coating into LSCF cathodes

4.8.1 Selection and Evaluation of Commercial Cells

We requested information and quotations for commercial cells from Materials and Systems Research, Inc. (MSRI), Nextech, H.C. Starck, and Delphi. We took into consideration different cell configurations (the anode-supported vs. electrolyte-supported cells), different cathode compositions (SDC barrier layer+LSCF cathode vs. SDC barrier layer+LSCF/SDC interlayer+LSCF cathode), and different cell sizes and active cathode areas. Table 2 shows detailed information of button cells we collected from several SOFC developers. In addition to our previous experience with the products of these companies, we believe that the price for each unit is an important factor of our final choice.

Company	Configuration	Size	Price for each at batch	Other
MSRI	Anode-supported; NiO/YSZ anode; SDC barrier layer; LSCF cathode;	• 27 mm for whole diameter • Active cathode area: 2 cm^2 (diameter:17.7 mm)	3 cells/$150 per cell; 20 cells/$125 per cell; 50 cells/$100 per cell; 100 cells/$80 per cell	With LSCF+SDC interlayer
Nextech	Anode-supported; NiO/YSZ anode; SDC barrier layer; LSCF cathode;	• 27 mm for whole diameter	3 cells/$750 per cell; 20 cells/$250 per cell	
H.C. Starck	Electrolyte-supported; 10Sc1CeSZ electrolyte; NiO/YSZ anode; SDC barrier layer; LSCF cathode;	• 25 mm for whole diameter • 20 mm for active cathode diameter	10 cells/$332 per cell	

Table 2 Detail information provided by three fuel cell suppliers.

We decided to select MSRI as our commercial cell supplier. Shown in Figure 14a are typical button cells we received. The button cell is 2.75 cm in diameter with an active cathode area of 2 cm^2. The cell configuration is a conventional anode (NiO/YSZ)-

supported electrolyte (YSZ) film. LSCF was used as the cathode material while SDC was employed as a barrier layer between electrolyte and cathode. LSCF/SDC was the cathode interlayer between LSCF and barrier layer. A cross-section of the MSRI cells is shown in Figure 14b. The thickness of the anode, electrolyte and cathode is estimated to be approximately 700 μm, 15 μm, and 70 μm, respectively.

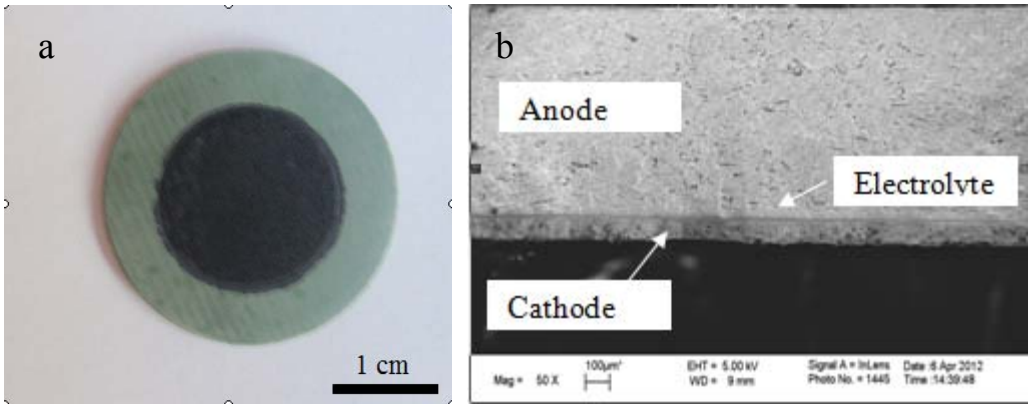

Figure 14 Typical button cells provided by MSRI: (a) Top view; (b) Crosssection view

We chose button cells rather than square cells with a larger size so that we could perform faster electrochemical testing (100 to 200 hours of operation) of infiltrated cells to use as feedback for parameter adjustment, which is the easiest and most effective way to evaluate our optimized infiltration process on large cells.

4.8.2 Optimization of Infiltration Process on MSRI Cells

As most of the infiltration process parameters have been optimized for homemade cells with a small cathode size (~ 0.3 cm^{-2}), the optimal values for infiltration should vary due to the difference in cathode microstructure between our homemade cells and the MSRI cells, such as the difference in grain size, grain size distribution, and pore size (Fig. 2 and 16). In particular, the larger cathode size would be more challenging for the solution infiltration to form a continuous and dense coating on the inner surface of the LSCF cathode, which is critical for the desired improvement in catalytic activity and stability of LSCF cathodes.

Firstly, we used the previous procedure for solution preparation and we found that the solution droplet did not easily spread out on the whole surface of LSCF cathode. We

thus changed the ratio of ethanol to water in the solution in order to reduce the surface tension of the solution. It turns out that the LSM droplet is able to distribute on the surface of LSCF cathode very well when the ratio of ethanol to water is increased to 2:1. However, further increase in ethanol proportion resulted in precipitation in solution, as shown in Figure 15.

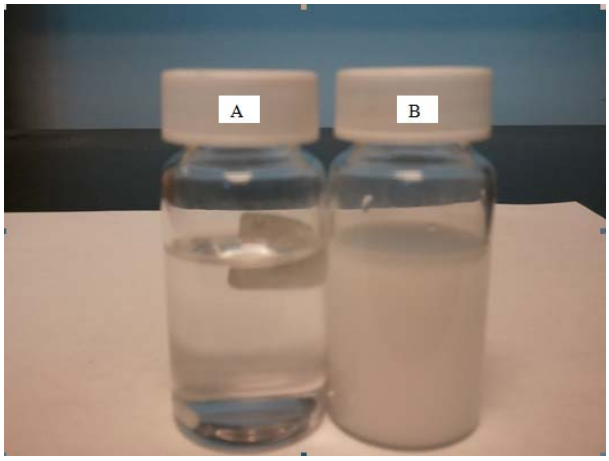

Figure 15 0.1 M LSM solution with different ratio of ethanol to water as solvent: a) 2:1; and b) 2.4:1.

We thus adjusted the pH value of the solution to 3.0. The solution was then stable at room temperature without precipitation during these three months. The effect of pH value of LSM solution on morphology and microstructure in LSM film on LSCF substrate has been investigated in detail in our 2010 Oct.-Dec. report.

With an increased ratio of ethanol to water in solution from 1:1 to 2:1, the 0.1 M infiltration solution appears to spread well on the cathode surface. However, we found that it is not successful when the solution concentration is further increased up to 0.3 M. Thus, we proposed a pre-infiltration thermal treatment process in which the cells were placed on a hot plate at 400^{o}C for 10 min and quenched down to room temperature before infiltration. The motivation of this process was to clean the LSCF cathode surface by removing some surface adsorbed species on the porous LSCF cathodes, such as moisture, CO_2, and other species from the ambient air. It is anticipated that, when the samples were heated up to 400^{o}C, the surface species were removed, thereby cleaning the surface of the LSCF cathode and improving its wettability. In general, after this heat treatment, the infiltration solution of higher concentration can easily wet the entire surfaces of the LSCF

cathode; the solution dropped on the top wicked into the porous electrode quickly. Without this thermal treatment, in contrast, the same solution drop would stay on the surface of the LSCF cathode.

Another issue is confining the infiltration solution to the surface of the cathode rather than the whole surface of the cell. This is very important to determine the amount of the solution that goes into the cathode backbone. We employed QPACs (poly-(alkylene) carbonates) as a sealant to prevent the solution from spreading too far. A QPAC glue was prepared through mixing QPAC and acetone at a weight ratio of 3:10, and then it was applied to the surface of the cell around the cathode area. After drying overnight, the QPAC glue completely solidified. After completing the infiltration process, the cells were fired at 900^{o}C for 1 hour to obtain the desired LSM phase. This process enables QPAC to decompose entirely. Note that QPACs are synthesized through the polymerization of carbon dioxide and epoxides. The products of their combustion are carbon dioxide and water vapor, which are non-toxic, non-flammable, and environmentally safe. They burn or evaporate cleanly in any environment, oxidizing or inert.

Since our optimal solution volume is 5 μL for homemade cell with an active cathode area of 0.3 cm^2, we employed different concentrations of LSM solutions with 35 μL, including 0.05 M, 0.1M and 0.3M to infiltrate into MSRI cells. Shown in Figure 16 are the SEM pictures of cross-sections of the LSCF cathode of the MSRI cells with and without LSM infiltration. The LSCF grains show a narrow size distribution and the size lies in the range of 100 to 200 nm. Similar to our previous observations in the homemade cells with infiltration, it is hard to observe formation of the dense LSM film or coating due to the structural similarity of LSM and LSCF. The visible difference is that the grains appear to have a smooth surface in blank LSCF cathode while the grain surface is obscured in all cases of the infiltrated LSCF cathodes, implying the formation of the LSM coating after infiltration.

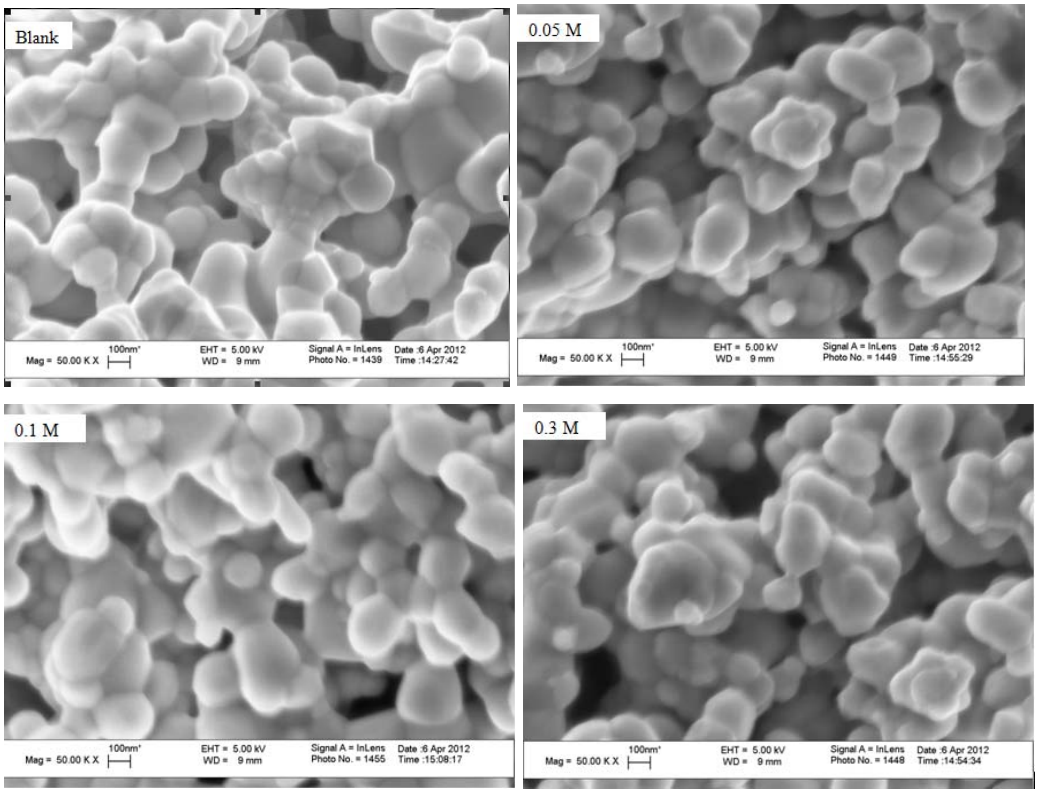

Figure 16 SEM pictures of cross-sections for the porous LSCF cathode of the MSRI cells infiltrated with different concentration of LSM solutions. The cathodes were annealed at 900^{o}C for 1 hour after infiltration.

4.8.3 Electrochemical Evaluation of MSRI Cells with LSM Infiltration at Short Term (100-200 hours)

As we indicated before, fast electrochemical testing (100 to 200 hours of operation) is the most effective method to evaluate infiltrated large cells and provides the best feedback for parameter adjustment. The electrolyte area of the cells purchased from MSRI is 5.91 ± 0.04 cm^2 and the active cathode area is 2.00 ± 0.03 cm^2.. Since the performance enhancement is closely associated with the concentration of the infiltration solution, electrochemical tests with different concentrations will provide information about optimizing the infiltration process. Shown in Figure 17 are the typical lifetimes of the MSRI cells with LSM solution infiltrations of different concentrations, measured at 750^oC at a constant voltage of 0.7 V. For comparison, the performance of a blank MSRI cell under the identical conditions is also listed, whose initial output power density is over 0.6 Wcm^{-2}. A gradual degradation over time is visible and the degradation rate is 0.025 % per hour. All of the LSM infiltrated MSRI cells exhibited a significant activation behavior. Although their initial output power density was slightly lower than the blank one (this tendency is very similar to our findings in the symmetrical cell as well as our modeling predictions from our 2010 Apr.-Jun. and Jul.-Sept. reports), the output increases very quickly with time and reaches a peak within the first 20 hours. Most importantly, the cell performance increases with solution concentration from 0.05 M to 0.3 M. This suggests that 0.3 M may be an optimal value for MSRI cells among the concentration range we studied.

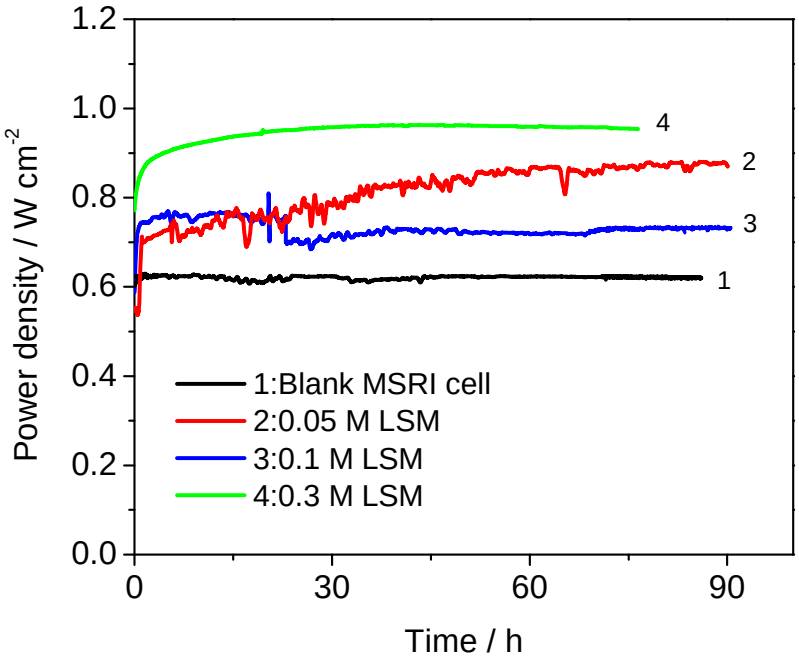

Figure 17 Power densities over time of the MSRI cells with LSM solution infiltrations of different concentrations at 750°C with a constant voltage of 0.7 V.

4.8.4 Construction of the New Multi-Cell Testing Stand

As discussion indicated in conference call on March 27, 2012, our original work plan has been adjusted slightly. Instead of sending infiltrated cells to PNNL for long-term testing, it was decided that GT should complete the demonstration in activity and stability enhancement of commercial cells using a homemade testing station. Therefore, we designed a new multi-cell testing stand which can test four cells simultaneously. Shown in Figure 18(a) is a cross-sectional view of the testing furnace, whose maximum temperature is 1100°C. An aluminum plate was also added on the bottom of the furnace, as shown in Figure 18(b), which is used as a holder for all four testing tubes. We also established an accompanying gas distribution system for the fuel supply, which features independent mass flow controllers and bubblers. After careful examination, safety considerations, and pre-operation testing, we were able to begin our long term performance tests.

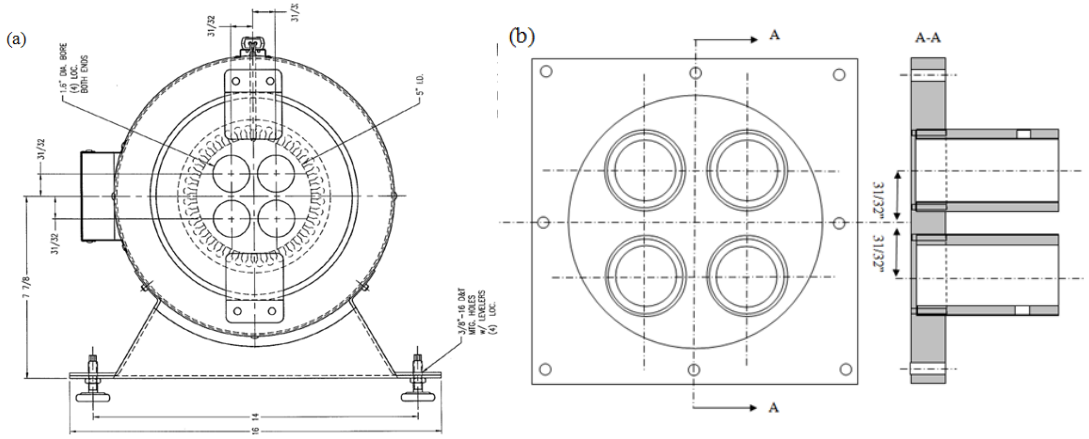

Figure 18 (a) Cross-sectional view of the homemade testing furnace that GT designed; and (b) top view of the aluminum holder for the four testing tubes.

4.5 Long-Term Stability Testing for the Infiltrated Cells on Our Custom Multi-cell Testing Stand.

After careful examination of the operation of the furnace, gas supply, and the bubblers to ensure that the individual parts are able to work well, we assembled two MSRI cells for pre-operation. During tens of hours of operation, the variation in temperature of the furnace was less than 0.2% and the variation in the gas flow was approximately 0.3%. More importantly, the performance in the cells contained reasonably small fluctuations. This indicated that the entire system was ready to be used for long-term testing of the infiltrated cells. Shown in Figure 19 is time dependence of the power density for a blank cell and three cells with 0.3 M LSM infiltration. The blank cell is referred to as Cell 1 and the other infiltrated cells are referred to as Cell 2, Cell 3, and Cell 4. Compared to the continuous and fast performance degradation in the blank cell during operation, all of the infiltrated cells show a significant activation process within the initial 30 to 40 hours of operation, followed by a slower degradation. For example, the degradation rates for Cell 2, Cell 3, and Cell 4 are 0.35%, 0.37%, and 0.37% (calculated based on when the maximum power density was achieved rather than the intial power density), compared with 0.51‰ for the blank cell. Thus, the performances of Cell 2, Cell 3, and Cell 4 are 24.1%, 33.9%, and 29.2% higher, respectively, than that of Cell 1 after 600-hour operation. This demonstrates that the LSM infiltration does enhance the activity and the stability of LSCF-based commercial cells of larger size. The cathode active area is 2.00 ± 0.03 cm^2 in the present case, which is about 7 times larger than the

cells made at GT. Noted that there is difference in cell performance, as seen in Fig. 17 and 19. This is because we used MSRI cells from two different batches. In the first batch, we used them for quick electrochemical characterization as feedback of our infiltration process optimization. In the second batch, the cells were used for long-term stability evaluation. All of our comparison was based on the same batch of the cells.

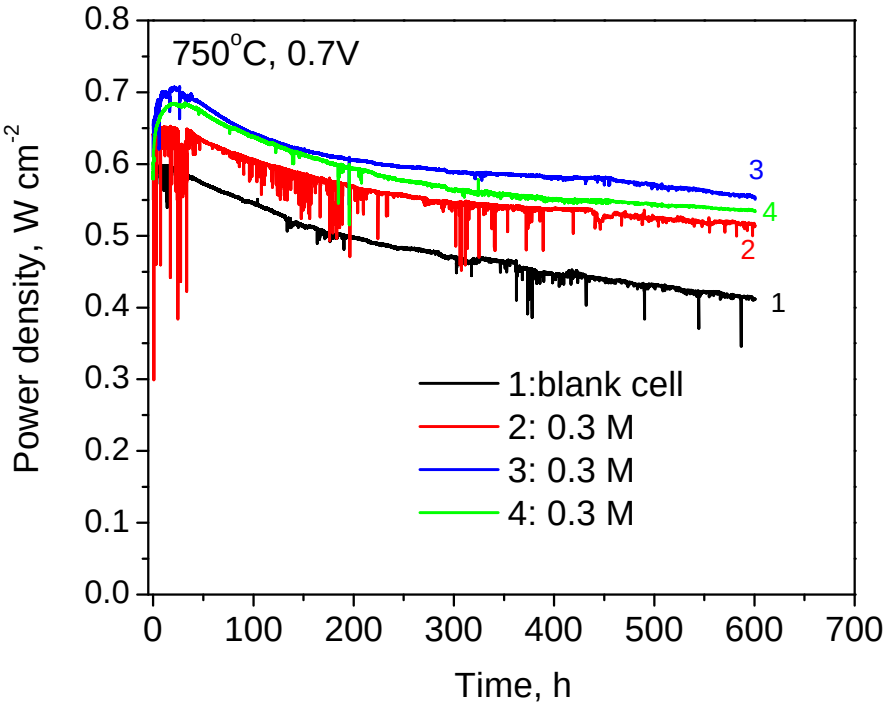

Figure 19 Power densities over time of four MSRI cells at 750°C with a constant voltage of 0.7 V: Cell1 was used as received (blank LSCF) while other 3 cells (Cell2, 3, and 4) were infiltrated with 0.3 M LSM solution of a fixed volume of 35 µL.

4.8.6 Post-Analysis of the MSRI Cells after Long-term Testing

4.8.6.1 SEM observation

After finishing the long-term testing, we carefully examined the microstructure of the tested MSRI cells. Shown in Figure 20 are SEM pictures of the whole cross-section for the LSCF cathode of the MSRI cells with and without LSM infiltration from the surface to the interface between the cathode and the buffer layer. Due to severe charging, the quality of the picture was significantly affected. However, it did not impact our local observation. We focused on three different areas including the top of LSCF cathode

(surface), the middle part of the cathode (bulk) as well as the innermost part (interface), which are labeled by blue, red, and green, respectively, in Figure 20. Unfortunately, it is still very hard to capture the detailed difference in microstructure between the blank and infiltrated cell, which implied that the thin film should form on the surface of the LSCF cathode instead of particles, and it did not cause significant changes in morphology and microstructure due to the structural similarity of LSM and LSCF [21, 22].

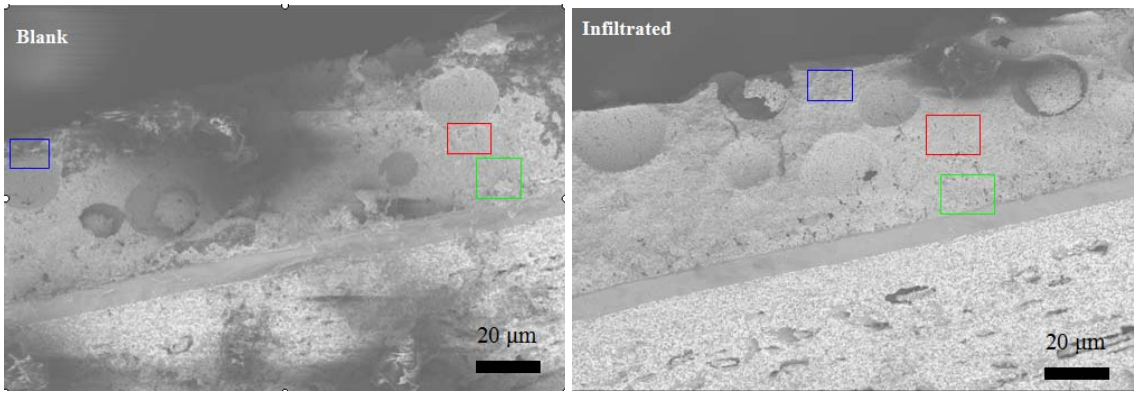

Figure 20 SEM pictures of the whole cross-section for LSCF cathode of MSRI cells with and without LSM infiltration after long-term testing.

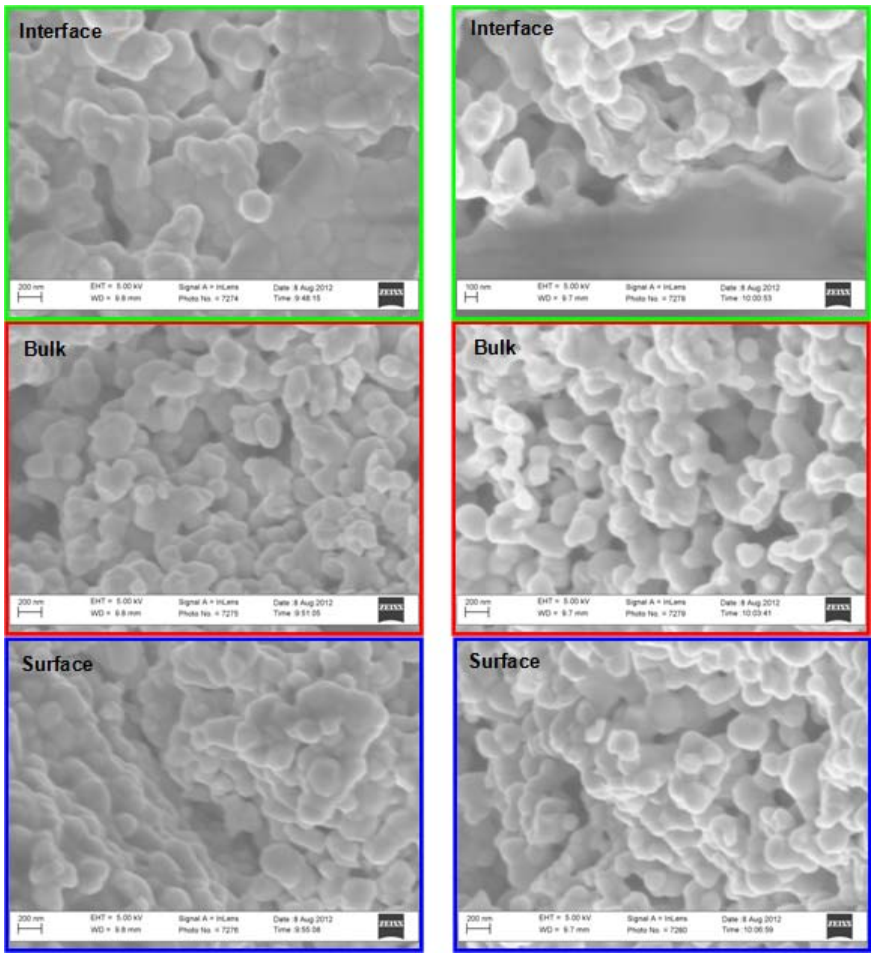

Figure 21 SEM pictures of the cross-section at different regions for LSCF cathode of MSRI cells with and without LSM infiltration after long-term testing (Left: the blank cell; Right: the infiltrated cell)

4.8.6.2 Raman analysis

Raman spectra were collected from various spots along the cross-section of the cathode (top surface to cathode/buffer layer interface) of an unmodified MSRI cell before and after operation. As shown in Figure 22(a), before the uninfiltrated cell was operated, the Raman spectrum only indicates a perovskite LSCF phase in the cathode as evidenced by the broad hump between 250 cm^{-1} and 800 cm^{-1} with a peak protruding at 550 cm^{-1}. After operation, however, small peaks emerged from the spectra that could correspond to trace amounts of secondary phase formation during operation (e.g., CoO_x). This secondary phase formation might be one reason for the cell's performance degradation. While the signal from these phases is obviously minute on these Raman spectra, future analysis by surface enhanced Raman spectroscopy might help to boost signal from these trace phases.

A cell with a cathode modified by LSM infiltration was analyzed in the same manner after operation, and Figure 22(b) shows the typical spectra obtained from this analysis. The characteristic Raman spectra for the modified cathode are similar to that of the unmodified cathode except for the large peak at 679 cm^{-1} in the modified cathode's typical spectrum, which is assigned to LSM. On the other hand, the small peaks present for the unmodified cathode after operation are not present for the modified cathode, indicating that the LSM modification staved off secondary phase formation. Finally, the ratio between the intensity of the peak at 679 cm^{-1} and the overall intensity of the broad 250-800 cm^{-1} hump was fairly constant across the cross-section of the cathode. The only exception to this was the spectrum collected closest to the buffer layer, shown in navy blue in Figure 22(b), where the ratio decreased slightly. Thus, the infiltration might have missed the "deepest" part of the cathode.

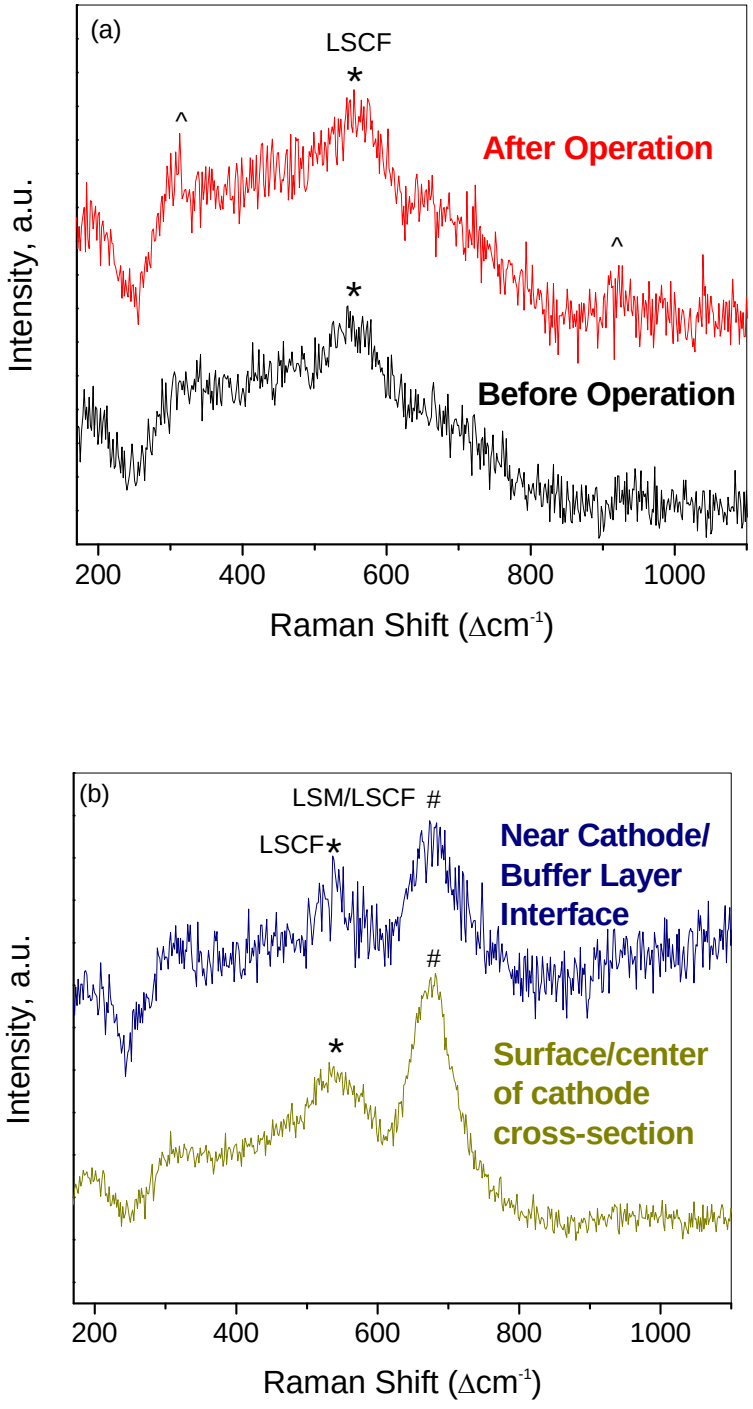

Figure 22 Raman spectra collected from the cathode of (a) a typical blank MSRI cell before and after operation; (b) 0.3 M LSM infiltration-modified cathode of a cell after operation.

5. CONCLUTIONS

We have successfully demonstrated that the activity and stability of LSCF cathodes can be improved by the introduction of a thin-film LSM coating through a simple and cost-effective solution infiltration process. We have also optimized the solution infiltration process for deposition of dense, conformal coatings of catalysts (e.g., LSM) with desired structure, composition, morphology, and thickness. Further, the surface and interface of blank LSCF cathodes without surface modification and LSM-coated LSCF cathodes were systematically characterized before and after electrochemical testing using advanced microscopy and spectroscopy techniques. TEM observation suggests that a layer of La and Sr oxide was formed on blank LSCF samples after annealing under conditions similar to fuel cell operation. Such surface oxide particles are expected to severely hamper the electrochemical activities of the electrodes. In contrast, the La/Sr oxide layer was not observable on LSM-coated LSCF samples after annealing under similar conditions. This is also consistent with our x-ray analyses. Soft x-ray XANES data reveal that Co cations displace the Mn cations as being more favored to be reduced. Variations in the Sr-O in the FT EXAFS for annealed LSCF samples suggest that some Sr segregation is occurring, but is not present in the annealed LSM-infiltrated LSCF cathode material. A surface enhanced Raman technique was developed and the signal enhancements were obtained for LSM and LSCF films on underlying YSZ substrate, enabling us to capture the surface information in perovskite-related cathodes. Electrochemical models for design of test cells and understanding of mechanisms were developed for the exploration of fundamental properties of electrode materials. Raman spectroscopy (e.g, SERS) and synchrotron-based x-ray analyses (e.g., XAS) are powerful techniques for probing electrode surfaces under various conditions. Together with the modeling and simulation tools developed earlier under this project, these characterization techniques may help us to unravel the mechanism of catalyst-infiltrated electrodes, thus providing scientific basis for rational design of more efficient cathode materials and structures. As a result, novel catalyst coatings through particle depositions (SDC, SSC, and LCC) were successively developed to decorate the LSCF cathode surfaces. Based on the knowledge we gained from LSM infiltration, continuous thin films (PSM and PSCM)

were developed to further improve the activity and stability of the LSCF cathodes. Finally, improved activity and stability of commercially available cells by an optimized LSM infiltration process were demonstrated over long periods of time. Microstructural examination of tested cells did not show visible differences between the blank and the infiltrated cells, suggesting that the infiltrated LSM may form a coherent film rather than discrete particles on the LSCF cathodes. There was no significant change in the morphology or microstructure of the LSCF cathode due to the structural similarity of LSCF and LSM. Raman analysis of the tested cells indicated small peaks emerging on the blank cells that correspond to trace amounts of secondary phase formation during operation (e.g., CoO_x). The formation of this secondary phase might be attributed to the performance degradation. In contrast, there was no such a secondary phase observed on the infiltrated cells, indicating that the LSM modification staved off secondary phase formation and thus improved the stability.

Publications

1. X. Li, K. Blinn, Y. Fang, M. F. Liu, M. Mahmoud, S. Cheng, L. Bottomley, M. El-Sayed and M. Liu, "*Application of surface enhanced Raman spectroscopy to the study of SOFC electrode surface*," Phys. Chem. Chem. Phys., 14, p. 5919-5923, 2012.
2. X. Li, K. Blinn, Y. Fang, M. Liu, M.A. Mahmoud, S. Cheng, L.A. Bottomley, M. El-Sayed, and M. Liu, "*Raman Spectroscopy Study of SOFC Electrode Surfaces*", Invited Talk Presented to the Symposium on In Situ Characterization of Fuel Cell Electrodes, MRS Fall Meeting, Boston, November 28-30, 2011.
3. D. Ding, M.F. Liu, Z.B. Liu, X. Li, K. Blinn, X.B Zhu, M. Liu, "*Efficient Electro-catalysts for enhancing surface activity and stability of SOFC cathodes."* Advanced Energy Materials, under review
4. M.F. Liu, D. Ding, K. Blinn, X.X. Li, L.F. Nie, and M.L. Liu, "*Enhanced performance of LSCF cathode through surface modification".* International Journal Of Hydrogen Energy, 2012. **37**(10): p. 8613-8620
5. Y. Bai, M. Liu, D. Ding, K. Blinn, W. Qin, J. Liu, and M. Liu, "*Electrical and electrocatalytic properties of a La0.8Sr0.2Co0.17Mn0.83O3-delta cathode for intermediate-temperature solid oxide fuel cells".* Journal of Power Sources, 2012. **205**: p. 80-85.
6. J. J. Choi, W. T. Qin, M. L. Liu, **"***Preparation and caracterization of* $(La_{0.8}Sr_{0.2})_{0.95}MnO_{3-\delta}$ *thin films and LSM/LSCF interface for SOFCs*", Journal of the American Ceramic Society, 2011. 94: p.3340–3345.
7. M. Liu, "*In Situ Characterization and Modeling of Surface and Interfaces in Fuel Cells*", Invited lecture, Lehigh University, September 14, 2011.
8. M. Liu, "*Surfaces and Interfaces in Heterogeneous Electrodes for Chemical and Energy Transformations*", Invited Talk to Symposium on Fuel Cells/Energy Conversion, MS&T2011, Columbus, OH, Oct. 18, 2011.
9. M. Liu, "*Rational Design of Materials for SOFCs*", Plenary Lecture presented to The Annual Meeting of Korean Ceramic Society, Gwangju, South Korea, October 24-25, 2011.
10. M. Lynch, L. Yang, W. T. Qin, J. J. Choi, M. F. Liu, K. Blinn and M. L. Liu, "*Enhancement of* $La_{0.6}Sr_{0.4}Co_{0.2}Fe_{0.8}O_{3-\delta}$ *durability and surface electrocatalytic activity by* $La_xSr_{1-x}Mn_8O_{3-\delta}$ *investigated using a new test electrode platform*", Energy and Environmental Science, In Press
11. M. Lynch and M. Liu, "*Investigation of Sheet Resistance in Thin-Film Mixed-Conducting SOFC Cathode Test Cells*," *J. Power Sources*, 195(16), 5155-5166, 2010.
12. X. Lou, Z. Liu, S. Wang, Y. Xiu, C.P. Wong, M. Liu, "*Controlling the morphology and uniformity of a catalyst-infiltrated cathode for SOFCs by tuning wetting property*," *J. Power Sources*, **195,** 419–424, 2010.
13. S. Lai, R. Rettew, M. Liu, C. Jaye, F. Alamgir, and M. Liu. "*In situ X-ray Absorption Spectroscopy for Solid Oxide Fuel Cell Cathodes."* HeteroFoaM All-Hands Meeting poster session, University of South Carolina, Columbia, SC USA, 2010.
14. L.F. Nie, M.F. Liu, Y.J. Zhang, and M. Liu, "$La_{0.6}Sr_{0.4}Co_{0.2}Fe_{0.8}O_{3-\delta}$ *Cathodes Infiltrated with Sm-Doped* CeO_2 *for SOFCs,*" Journal of Power Sources, 195(15), 4704-4708, 2010.

15. Z. Liu, Z. W. Zheng, M. F. Han, et al., "*High performance SOFCs based on tri-layer YSZ by low temperature sintering process*", Journal of Power Sources, **195**, 7230-7233, 2010.
16. L. F. Nie, Z. Liu, M. F. Liu, L. Yang, Y. Zhang, and M. Liu, "*Enhanced Performance of $La_{0.6}Sr_{0.4}Co_{0.2}Fe_{0.8}O_{3-\delta}$ Cathodes with Graded Microstructure Fabricated by Tape Casting*", Journal of Electrochemical Science and Technology, **1**(1), 50-56, 2010.
17. M. Lynch, X. Li, L. Yang, D. Mebane, M. Liu, "*Investigation of SOFC Cathode Kinetics by Means of Continuum Modeling and Well-Defined Electrodes*," 217th Meeting of The Electrochemical Society, Vancouver, British Columbia, Canada, April 2010.'
18. X. Li, M. Lynch, M.F. Liu, X. Lou, M. Liu, "*Investigating Catalytic Properties of Cathode Materials Using Patterned Electrodes*," 217th Meeting of The Electrochemical Society, Vancouver, British Columbia, Canada, April 2010.
19. M.E. Lynch, D.S. Mebane, Y.M. Choi, and M. Liu, "*Numerical Continuum Modeling of Thin Film Solid Oxide Fuel Cell Cathode Materials*," (invited) International Center for Materials Research Workshop on Modeling of Fuel Cell Electrocatalysts, Santa Barbara, California, USA, July 2009.

References

1. Minh, N.Q., *Ceramic Fuel-Cells.* Journal of the American Ceramic Society, 1993. 76(3): p. 563-588.
2. Steele, B.C.H. and A. Heinzel, *Materials for fuel-cell technologies.* Nature, 2001. 414(6861): p. 345-352.
3. Liu, M., et al., *Rational SOFC material design: new advances and tools.* Materials Today, 2011. 14(11): p. 534-546.
4. Singhal, S.C., *Solid oxide fuel cells for stationary, mobile, and military applications.* Solid State Ionics, 2002. 152: p. 405-410.
5. Fleig, J., *Solid oxide fuel cell cathodes: Polarization mechanisms and modeling of the electrochemical performance.* Annual Review of Materials Research, 2003. 33: p. 361-382.
6. Murray, E.P., T. Tsai, and S.A. Barnett, *Oxygen transfer processes in (La,Sr)MnO3/Y2O3-stabilized ZrO2 cathodes: an impedance spectroscopy study.* Solid State Ionics, 1998. 110(3-4): p. 235-243.
7. Jiang, S.P., *A comparison of O-2 reduction reactions on porous (La,Sr)MnO3 and (La,Sr)(Co,Fe)O-3 electrodes.* Solid State Ionics, 2002. 146(1-2): p. 1-22.
8. Simner, S.P., et al., *Degradation mechanisms of La-Sr-Co-Fe-O3SOFC cathodes.* Electrochemical and Solid State Letters, 2006. 9(10): p. A478-A481.
9. Lane, J.A., et al., *Oxygen transport in La0.6Sr0.4Co0.2Fe0.8O3-delta.* Solid State Ionics, 1999. 121(1-4): p. 201-208.
10. Ding, D., et al., *High reactive Ce0.8Sm0.2O1.9 powders via a carbonate co-precipitation method as electrolytes for low-temperature solid oxide fuel cells.* Solid State Ionics, 2008. 179(21-26): p. 896-899.
11. Ding, D., et al., *Electrical properties of samaria-doped ceria electrolytes from highly active powders.* Electrochimica Acta, 2010. 55(15): p. 4529-4535.
12. Liu, M.F., et al., *Enhanced performance of LSCF cathode through surface modification.* International Journal of Hydrogen Energy, 2012(doi:10.1016/j.ijhydene.2012.02.139).
13. Choi, Y.M., et al., *Characterization of O-2-CeO2 interactions using in situ Raman spectroscopy and first-principle calculations.* Chemphyschem, 2006. 7(9): p. 1957-1963.
14. Yang, L., et al., *Enhanced Sulfur and Coking Tolerance of a Mixed Ion Conductor for SOFCs: BaZr0.1Ce0.7Y0.2-xYbxO3-delta.* Science, 2009. 326(5949): p. 126-129.
15. Li, X., et al., *Application of surface enhanced Raman spectroscopy to the study of SOFC electrode surfaces.* Physical Chemistry Chemical Physics, 2012.
16. Ding, H., et al., *Suppression of Sr surface segregation in La1-xSrxCo1-yFeyO3-δ: A First Principles Study.* Physical Chemistry Chemical Physics, 2012(doi:10.1039/C2CP43148C).
17. Ishihara, T., et al., *Doped Prmno3 Perovskite Oxide as a New Cathode of Solid Oxide Fuel-Cells for Low-Temperature Operation.* Journal of the Electrochemical Society, 1995. 142(5): p. 1519-1524.

18. Ishihara, T., H. Matsuda, and Y. Takita, *Doped Lagao3 Perovskite-Type Oxide as a New Oxide Ionic Conductor.* Journal of the American Chemical Society, 1994. 116(9): p. 3801-3803.
19. Kostogloudis, G.C. and C. Ftikos, *Oxygen nonstoichiometry in Pr1-xSrxCo0.2B0.8O3-delta (B = Mn, Fe, x=0.2, 0.4) perovskite oxides.* Journal of the European Ceramic Society, 2007. 27(1): p. 273-277.
20. Sun, C., R. Hui, and J. Roller, *Cathode materials for solid oxide fuel cells: a review.* Journal of Solid State Electrochemistry. 14(7): p. 1125-1144.
21. Lynch, M.E., et al., *Enhancement of La(0.6)Sr(0.4)Co(0.2)Fe(0.8)O(3-delta) durability and surface electrocatalytic activity by La(0.85)Sr(0.15)MnO(3 +/-delta) investigated using a new test electrode platform.* Energy & Environmental Science, 2011. 4(6): p. 2249-2258.
22. Choi, J.-J., et al., *Preparation and Characterization of (La(0.8)Sr(0.2))(0.95)MnO(3-delta) (LSM) Thin Films and LSM/LSCF Interface for Solid Oxide Fuel Cells.* Journal Of The American Ceramic Society, 2011. 94(10): p. 3340-3345.

Acronyms

SOFC: solid oxide fuel cell
YSZ: yttria-stabilized zirconia
SDC: samarium doped ceria with chemical formula $Sm_{0.2}Ce_{0.8}O_{1.95-\delta}$
LSM: the cathode material with chemical formula $La_xSr_{1-x}MnO_{3-\delta}$
LSCF: the cathode material with chemical formula $La_{0.6}Sr_{0.4}Co_{0.2}Fe_{0.8}O_{3-\delta}$
SSC: the cathode materials with chemical formula $Sm_{0.5}Sr_{0.5}CoO_{3-\delta}$
LCC: the cathode material with chemical formula $La_{0.4875}Ca_{0.0125}Ce_{0.5}O_{2-\delta}$
PSM: the cathode material with chemical formula $Pr_xSr_{1-x}MnO_{3-\delta}$
PSCM: the cathode material with chemical formula $PrSrCoMnO_{6-\delta}$
XRD: x-ray diffraction
SEM: Scanning electron microscopy
TEM: Transmission electron microscopy
SERS: surface enhanced Raman spectroscopy
XAS: x-ray absorption spectroscopy
XANES: x-ray absorption near-edge spectroscopy
EXAFS: extended x-ray absorption fine structure
FT: Fourier-transformed
OCV: open circuit voltage
ORR: oxygen reduction reaction
R_p: interfacial polarization resistance
MSRI: Materials System and Research, Incorporated